MARMARA UNIVERSITY
INSTITUTE FOR GRADUATE STUDIES IN PURE AND APPLIED SCIENCES

MATHEMATICAL MODELLING OF HYDRATION OF CALCIUM OXIDE (CaO) IN A PACKED BED CHEMICAL HEAT STORAGE UNIT

ENDER ERCAN

MASTER THESIS
Department of Chemical Engineering

Thesis Supervisor
Assoc. Prof. Kurtul Küçükada

ISTANBUL, 2015

MARMARA UNIVERSITY
INSTITUTE FOR GRADUATE STUDIES IN PURE AND APPLIED SCIENCES

MATHEMATICAL MODELLING OF HYDRATION OF CALCIUM OXIDE (CaO) IN A PACKED BED CHEMICAL HEAT STORAGE UNIT

ENDER ERCAN

MASTER THESIS
Department of Chemical Engineering

Thesis Supervisor
Assoc. Prof. Kurtul Küçükada

ISTANBUL, 2015

MARMARA UNIVERSITY
INSTITUTE FOR GRADUATE STUDIES IN PURE AND APPLIED SCIENCES

Ender ERCAN, a Master of Science student of Marmara University, Institute for Graduate Studies in Pure and Applied Sciences, defended his thesis entitled "**Mathematical modeling of hydration of calcium oxide (CaO) in a packed bed chemical heat storage unit**", on ..January 12, 2015... and has been found to be satisfactory by the jury members.

Jury Members

Assoc. Prof. Kurtul KÜÇÜKADA (Advisor)
Marmara University .....

Assoc. Prof. Emre ALPMAN (Jury Member)
Marmara University .....

Assist. Prof. Neslihan ALEMDAR (Jury Member)
Marmara University .....

APPROVAL

Marmara University Institute for Graduate Studies in Pure and Applied Sciences Executive Committee approves that Ender ERCAN be granted the degree of Master of Science in Department of Chemical Engineering Program on 26.01.2015 ..... (Resolution no: 2015/03-02).

Director of the Institute

Prof. Dr. Uğur YAHŞİ

ACKNOWLEDGEMENT

During completion of my master thesis I owe a debt of gratitude to many people who helped and supported me. First of all, I would like to express my deep gratitude to Dr. Kurtul Küçükada who has provided me many valued advises, encouragements, assistances and kind supports during my research time and my master education.

I am also thankful to all of friends who always accompany me and cheer me up. I wish to express appreciation to my mom and dad who always give me so much supports and love. They always encouraged me to continue my education further and kept their constant source of enthusiasm, not only during this thesis project but also during all my life. I am forever thankful to Charlene, for her endless patience and encouragement. Thank you very much to all of you.

Last, I would like to thank the Institute for Graduate Studies in Pure and Applied Sciences, Marmara University for their elegant education system in Istanbul. I would like to thank the respective departments of Marmara University for Master program.

LIST OF CONTENTS

ABSTRACT

MATHEMATICAL MODELING OF HYDRATION OF CALCIUM OXIDE (CaO) IN A PACKED BED CHEMICAL HEAT STORAGE UNIT

In 21st century, renewable energy sources become the most important research area of humanity. Increasing of the human population and thus energy requirement causes the energy consumption to increase. Therefore many investigators have been focused on renewable energy technologies. Thermal energy storage is one of technologies that promising a clean energy technology of future.

There are three main aspects to store energy using thermal energy technologies. Sensible heat storage involves storing or extracting energy through a solid or liquid material without phase change for a given temperature interval. Latent heat using phase change materials release or store energy when the materials phase change. Chemical energy storage is the most innovative and powerful one that can store the thermal energy owing to the chemical bounds of reversible reactions. The chemical heat storage units may be used to supply high temperature heat requirements. Hydration of CaO has recently been intensively studied as chemical heat storage medium due to its high potential such as availability and price.

The aim of this work is mathematical modeling of a thermochemical energy storage using hydration reaction of CaO. During hydration reaction, water vapor reacts with CaO particles and releases energy. Present thesis mostly focuses on direct concept of thermochemical energy storage using CaO. The simulations were performed by the solution of the model equations simultaneously concerning the reaction kinetics and heat transfer phenomena. There are two approaches to investigate thermochemical energy storage. These are lumped and distributed parameter models. The lumped parameter model (LPM) was developed for a closed system where variables were considered to be a function of time only and model equations were solved using Euler's method. On the other hand, the distributed parameter model (DPM) was developed for the open system where variables were considered to be a function of time and axial position of thermochemical energy storage (TCES) unit. Model equations were partial differential equations and solved using

finite difference method. Numerical solution of mathematical model equations were done using Matlab ® software. Simulations were performed for different design and operating parameters of thermochemical energy storage unit using CaO.

ÖZET

DOLGULU YATAKLI KiMYASAL ISI DEPOSUNDA KALSiYUM OKSiTiN (CaO) HiDRASYONUNUN MATEMATiKSEL MODELLENMESi

21. yüzyılda yenilenebilir enerji kaynakları insanlığın en önemli konusu haline gelmiştir. Artan insan nüfusunun sonucu doğan enerji kullanımı, enerji ihtiyacının artmasına neden olmuştur. Bunun bir sonucu olarak araştırmacılar yeni enerji kaynakları ve enerji depolama üzerine yoğunlaşmışlardır. Termal enerji depoları bunların gelecekte en güven verecek potansiyele sahip olanıdır. Termal enerji depoları enerji depolama açısından üç ana başlık altında toplanmıştır. Duyulur ısı depoları enerjinin sıvı yada katı dolgu maddelerinden faz değiştirmeksizin depolanması ve serbest bırakımı prensibine dayanır. Gizli ısı depolarında ise faz değiştiren maddelerin vasıtasıyla enerji depolama ve geri kazanım işlemi gerçekleşmektedir. Kimyasal enerji depoları içlerinde en yenilikçi olan ve gelecek için güven veren teknolojidir. Kimyasal ısı depolarında enerji tersinir reaksiyonlar vasıtasıyla kimyasal bağlar içerisinde depolanır.

Bu çalışmanın temel amacı ısı transferi mekanizması iletim, adveksiyon ve konveksiyon ile yürüdüğü durumda kalsiyum oksitin (CaO) dolgulu yaktaklı ısı deposu tanklarında sıcaklık dağılımının belirlenmesi ve su buharı debisi gibi bazı değişkenlerin sıcaklık dağılımına etkisidir. Model geliştirilirken birleştirilmiş ve dağıtılmış parametreli olarak iki değişik yol izlenmiştir. Birleştirilmiş parametreli model sadece zaman değişkeni göz önüne alınarak direk konseptli kapalı bir sistem için elde edilmiştir ve model denklikleri Euler metodu yardımıyla çözülmüştür.

Diğer yandan dağıtılmış parametreli model hem reaktör yüksekliği hem de bağımsız değişken olan zamanın fonksiyonu olarak açık sistem için geliştirilmiştir. Model denklikleri sonlu farklar yöntemi ile çözülmüştür. İleri sürülen matematiksel modelin nümerik çözümü Matlab ® yazılımı kullanılarak gerçekleştirilmiştir. Simülasyonlar değişik tasarım ve çalışma koşulları için denenmiştir.

SYMBOLS

a	**:** Spesific heat transfer area	(m^2 / m^3)
A	**:** Pre-exponential factor	(1 / s)
A_c	**:** Cross sectional area	(m^2)
C	**:** Concentration	(mol / m^3)
C [%]	**:** Conversion	(kg / kg)
c_p	**:** Heat capacity	(J / kg . K)
d	**:** Particle diameter	(m)
D	**:** Reactor diameter	(m)
E	**:** Activation energy	(J / mol)
G	**:** Gibbs free energy	(J)
h	**:** Convective heat transfer coefficient	(W / m^2 . K)
H	**:** Enthalpy	(J)
K	**:** Reaction rate constant	(-)
k	**:** Thermal conductivity	(W / m . K)
k_h	**:** Hydration reaction rate constant	(1 / s)
L	**:** Height	(m)
m	**:** Mass	(kg)
$\dot{m}$	**:** Mass flow	(kg / s)
M_w	**:** Molecular weight	(kg / mol)
n	**:** Mol	(mol)
P	**:** Pressure	(atm)
Q	**:** Heat	(J)
$\dot{Q}$	**:** Heat flow	(J / s)
R	**:** Universal gas constant	(J / mol . K)
r	**:** Reaction rate	(mol / m^3. s)
S	**:** Entropy	(J / K)
T	**:** Temperature	(K)
t	**:** Time	(s)
V	**:** Volume	(m^3)
ϑ	**:** Velocity	(m / s)
X	**:** Conversion	(-)

Greek Symbols

Δ	**:** Change of a dimension	
$\boldsymbol{\varepsilon}$	**:** Emissivity Coefficient	(-)
$\boldsymbol{\sigma}$	**:** Stefan-Boltzman Constant	($W / m^2 K^4$)
ρ	**:** Density	(kg / m^3)
ε	**:** Porosity	(-)
$\boldsymbol{\lambda}$	**:** Latent heat	(kj / kg)

Dimensionless numbers

Nu	**:** Nusselt number	(h D / k)
Re	**:** Reynolds number	(ρ v d / μ)

Subscripts

av	**:** Average
D	**:** Dehydration
eq	**:** Equilibrium state
f	**:** Fluid
g	**:** Gas
H	**:** Hydration
in	**:** Inlet
l	**:** Liquid
out	**:** Outlet
R	**:** Reaction
s	**:** Solid
vap	**:** Vapor

ABBREVIATIONS

TES **:** Thermal Energy Storage

TCES **:** Thermo-chemical Energy Storage

DPM **:** Distributed Parameter Model

LPM **:** Lumped Parameter Model

SHS **:** Sensible Heat Storage

HTF **:** High Temperature Fluid

DSC **:** Differential Scanning Calorimetry

PCM **:** Phase Change Material

1D **:** One Dimensinional

CaO **:** Calcium Oxide

MgO **:** Magnesium Oxide

CaOH **:** Calcium Hydroxide

LIST OF FIGURES

LIST OF TABLES

CHAPTER 1

INTRODUCTION

The limitation, price and environmental issues related to the fossil fuels forces investigators to develop alternatives such as using the renewable energy sources. Some examples of renewable energy sources are solar energy, wind energy, and ground energy. The efficient use of the renewable energy sources requires the storage of the energy. When talking about energy storage in fact there are two concepts which should be discussed separately being electric energy storage and thermal energy (heat) storage. The aim of the present thesis concerns the thermal energy storage and more specifically thermo-chemical energy storage. In the following sections and subsections of the present chapter, thermal energy storage methods will be briefly outlined following a more detailed analysis of the thermo-chemical energy storage.

1.1. Heating and Energy Requirements

Eskin and Türkmen (2008) reported that the average annual required energy per floor area of a building was predicted to be between 340-428 kWh/m^2 depending on the location of the city. Another similar work presented by Evcil (2012), reported that the average residential space heating requirement in Turkey was around 17 GJ/year residence. In one of the recent studies, Kazanasamaz et al. (2014) reported that the real heating energy consumption in residential buildings ranged between 100 and 200 kWh/m (the average is obtained as 175 kWh/m^2) in Turkey.

In the report of Department of Energy and Climate Change of the U.K. government (2013), it was stated that 66% of the total energy requirement of domestic energy consumption is for space heating. In the same report it was also presented that in 2011, the gas consumption in UK was estimated to be 15,257 kWh .

1.2. Heat Storage Methods

The thermal energy or heat can be stored using three main methods such as sensible heat, latent heat and thermo-chemical energy storage methods. In this section, the

thermal energy storage methods will briefly be presented. Thermal energy storage methods are shown in Figure 1.1.

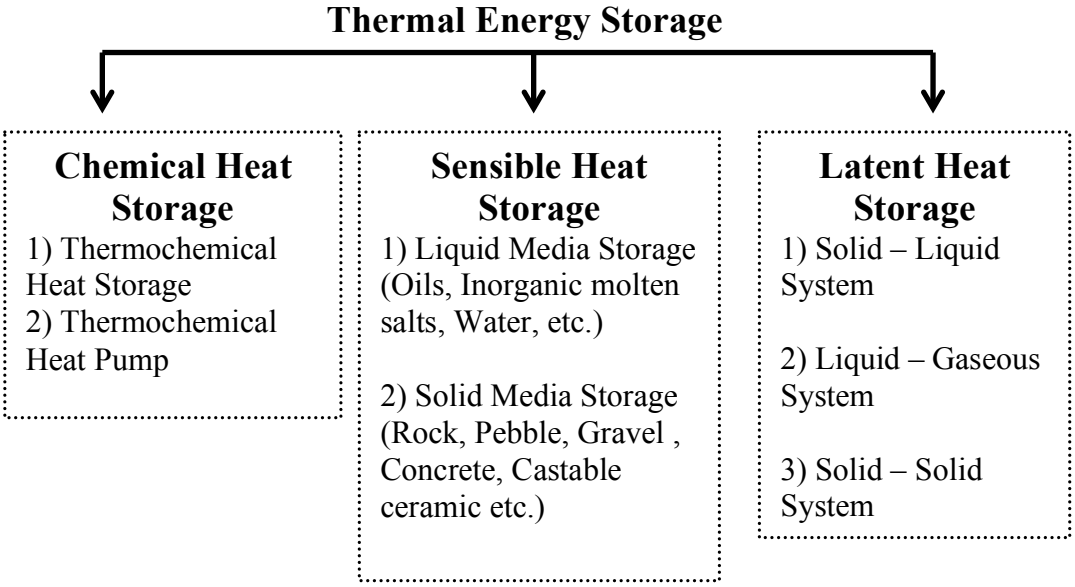

Figure 1.1. Overview of Thermal Energy Systems

1.2.1. Sensible Heat Storage

Sensible heat storage involves storing or extracting energy through a solid or liquid without changing phase. In sensible heat storage, the energy content corresponds to the temperature change in liquid or solid storage material which is mostly used as water, air, oil, rock beds, bricks, sand, or soil (Dinçer and Rosen, 2011).

Amount of heat supplied to the sensible heat storage unit depends on various factors such as final and initial temperatures; the mass of storage medium and material's heat capacity. All mediums have different thermo-physical properties, advantages and disadvantages. For example, water has a specific heat that is two times higher than specific heat of rock or soil. Common media materials to be used in sensible thermal (heat) and latent heat storages are shown in Table 1.1.

The heat capacity of the medium and the range of the temperature change can be represented as in the following equation;

$$Q_S = \int_{T_1}^{T_2} m.C_p.dT = m.C_{p(av)}.(T_2 - T_1) \qquad (1.1)$$

Q_S = Sensible heat stored, kJ

T_1 = Initial temperature, °C

T_2 = Final temperature, °C

m= Mass of heat storage medium, kg

C_p = Specific heat, kJ/kg.°C

$C_{p(av)}$ = Average specific heat between T_1 and T_2, kJ / kg.°C

Table 1.1. Available media for sensible and latent thermal energy storage systems, Dinçer and Rosen (2011).

Sensible Short term	Sensible Long term (annual)	Latent Short term
Rock beds	Rock beds	Inorganic materials
Earth beds	Earth beds	Organic materials
Water tanks	Large water tanks	Fatty acids
-	Aquifers	Aromatics
-	Solar ponds	-

1.2.2. Latent Heat Storage

Latent heat is the energy that is released when a material undergoes the phase changes such as melting, evaporation and crystallization. For example, when water is boiled the latent heat of evaporation is carried by the steam produced. The materials used for storing latent heat, are defined as phase change materials (PCMs). Examples of PCMs can be given as water/ice, paraffin and eutectic salts such as; palmitic and stearic acids, and nitrate salts. When the phase change material is heated above its melting point, the chemical bonds within the PCM break up from solid to liquid phase. Due to phase change as an endothermic process, the phase change material absorbs thermal energy. As the environment cools down, the phase change material will return to solid phase and gives off the absorbed heat. PCMs are supplied mostly in the shape as powder, granulate and board. The process is shown in Figure 1.2. The

amount of energy stored is due to the amount of phase change material and the latent heat of phase change material and it can be represented as;

$$Q_L = m.\lambda \tag{1.2}$$

Q_L = Latent heat stored kJ

m = The mass of PCM, kg

λ = Latent heat of PCM, kJ/kg

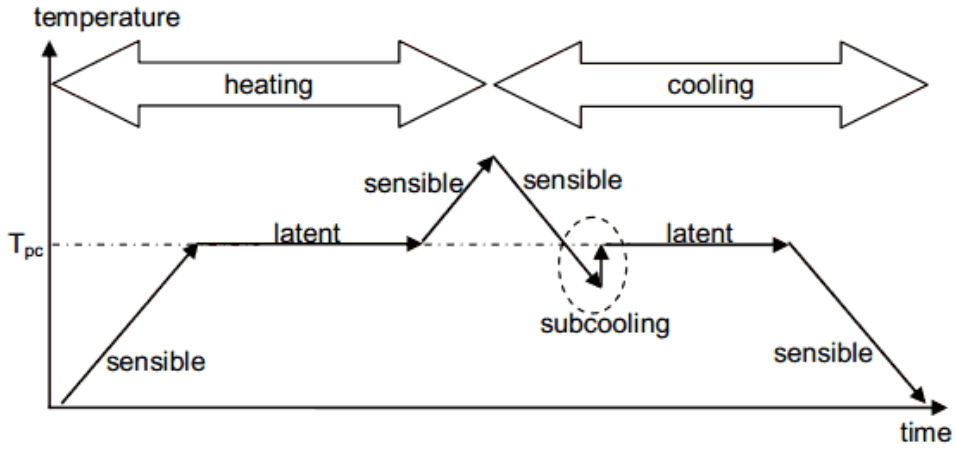

Figure 1.2. Diagram of the heating and cooling (charging and discharging) process with subcooling for latent heat (Mehling and Cabeza, 2008).

Fig 1.2 clearly indicates that temperature change of a latent energy storage during charging (melting) and discharging (solidification). This process takes place consecutively in a latent heat storage unit using phase change material. T_{pc} as seen in Fig 1.2, means the appropriate phase temperature to release and store energy by means of latent heat.

The subcooling process is a necessary application for a latent heat storage. In this case subcooling is meant the temperature difference between the temperature of the melting point, and the actual temperature of solid. Therefore the heat is released and material begins to solidify. This effect is also known as supercooling. If the temperature under the melting point is not reached, the phase change material will not completely solidify. Thus, storage unit can only store the sensible heat.

1.2.3. Chemical Heat Storage

Chemical heat storage can store the thermal energy owing to the chemical bounds of reversible reactions. There are two ways to provide energy to a thermochemical energy storage (TCES) such as sorption and thermo-chemical reactions. The sorption process includes absorption and adsorption. When TCES is to be considered, absorption can be defined as gas phase enters a liquid absorbent. Furthermore, absorption takes place when a substance is dispersed in liquid and solid or forms of a solution, Abedin and Rosen (2012).

The principle of TCES is based on using the enthalpy of reaction. When the chemical compound is heated, two separate components are formed and the reaction heat is stored. As a result, these two components can react again and release the heat of reaction. The TCES capacity depends on the heat of the reaction and free energy of the reaction (Çengel and Boles, 2012).

In the present thesis, the reaction of CaO hydration is considered. Hence the hydration reaction of CaO can be given as follows;

$$CaO_{(s)} + H_2O_{(v)} \longrightarrow Ca(OH)_{2\,(aq)}$$

The thermal energy to be stored in a chemical heat storage unit depends on the molar quantity of the reactant and the reaction enthalpy can be represented as;

$$Q = n_A.\Delta H_R \tag{1.3}$$

In addition, the effect of the sensible heat storage capacity of the chemical heat storage unit plays an important role in determining the dynamic behavior during charging (storage) and discharging (recovery) periods. Next chapter will present the detailed information concerning the chemical heat storage and more specifically information concerning the details and current investigations on the chemical heat storage methods will be outlined.

CHAPTER 2

CHEMICAL HEAT STORAGE

Chemical heat storage has the highest potential to store energy by means of using the heat of a reversible chemical reaction when it is compared with other types of heat storage methods such as sensible and latent heat storage methods. The advantage of thermo-chemical heat storage is not only the highest heat storage capacity but also its other inviting feature such as its energy conservation potential at ambient temperature as long as desired without any heat loss. The chemical heat storage systems work using the energy required and released during the destruction and production of the chemical bonds.

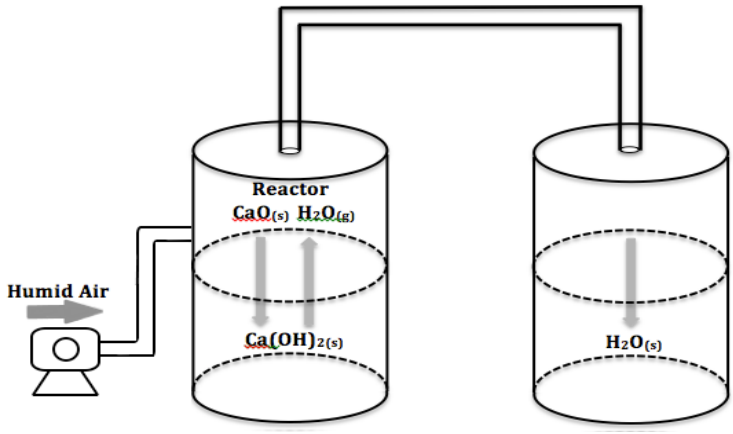

Figure 2.1. Diagram of the TCES by using CaO/Ca(OH) reaction

Figure 2.1 is a suggested design of the thermochemical energy storages and it clearly shows hydration and dehydration of CaO takes place in a unit. When humid air supplies in TCES unit, the hydration reaction occurs and heat is released. Contrary, when dehydration reaction of CaO takes place in TCES unit, water becomes unbound and accumulates in other tank.

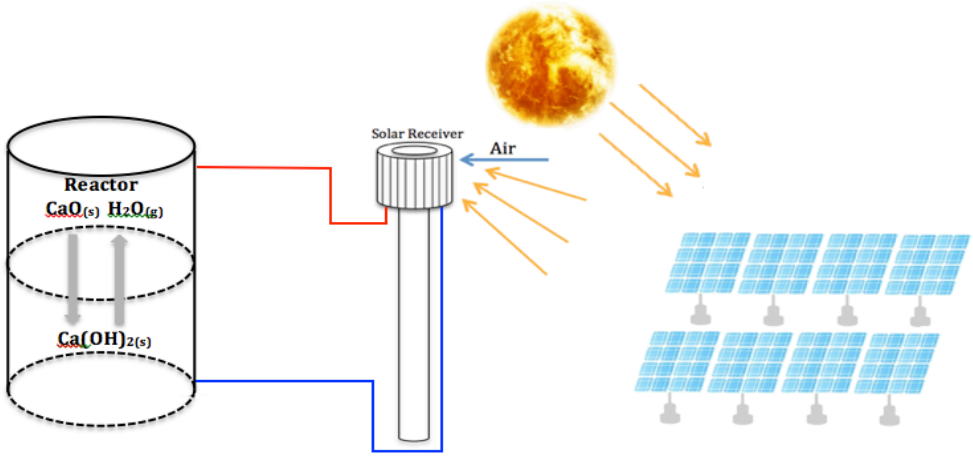

Figure 2.2. A future concept for thermochemical heat storage by using CaO/Ca(OH) reversible reaction modified with concentrated solar power field.

Figure 2.2 shows the desired TCES units combined with the solar thermal energy field. During the dehydration, the TCES unit requires external energy to reach temperatures above the equilibrium temperature of the reversible reaction. Moreover there is lack of improvement of the energy storing in the electric energy storage systems by using the solar energy. It is possible that concentrated solar panel technology will be available to use together with thermochemical energy storage system in order to store solar energy.

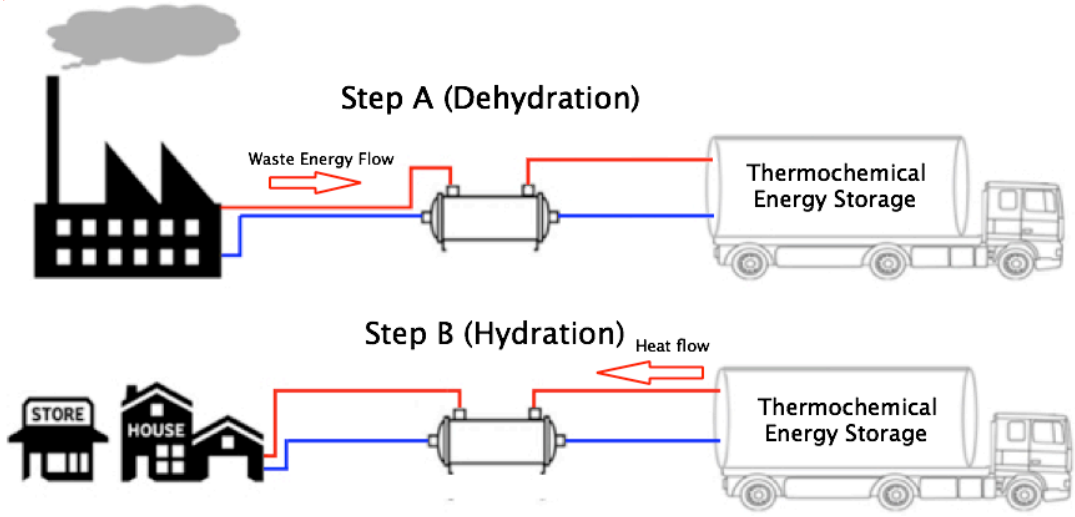

Figure 2.3. Schematic flow chart representing the storage of waste heat and the use of the stored thermochemical energy for residential purpose.

The use of waste heat for TCES, delivery and the discharge of the stored heat are all depicted in Fig. 2.3. As it can be seen on Fig. 2.3, in step A, the waste heat was stored by the chemical energy storage unit, located at the truck hauler. In step B, the figure shows the release of the stored heat for municipal use.

2.1. Chemical heat storage materials and methods

The three main classes of reactions having the potential of being used for chemical heat storage are the hydration/dehydration of metal oxides, carbonation/decarbonation of metal carbonates and hydration/dehydration of salt hydrates. Some reactions occurring in thermo-chemical heat storage systems are represented in Table 2.1.

Table 2.1. Selection of potential reactions for chemical heat storage (adapted from Kerskes et al., 2011).

	Reaction	**Temperature[°C]**
Dehydration of metal oxides	$Mg(OH)_2 \Leftrightarrow MgO + H_2O$	250-350
	$Ca(OH)_2 \Leftrightarrow CaO + H_2O$	450-550
	$Ba(OH)_2 \Leftrightarrow BaO + H_2O$	700-800
Decarbonation of metal carbonates	$ZnCO_3 \Leftrightarrow ZnO + CO_2$	100-150
	$MgCO_3 \Leftrightarrow MgO + CO_2$	350-450
	$CaCO_3 \Leftrightarrow CaO + CO_2$	850-950
Dehydration of salt hydrates	$MgSO_4 \cdot 7H_2O \Leftrightarrow MgSO4 \cdot H_2O + 6H_2O$	100-150
	$MgCl_2 \cdot 6H_2O \Leftrightarrow MgCl_2 \cdot H_2O + 5H_2O$	100-130
	$CaCl_2 \cdot 6H_2O \Leftrightarrow CaCl_2 \cdot H_2O + 5\ H_2O$	150-200

In this table, three main categories of the chemical reactions and their temperature ranges are listed. The temperature range varies from 100 to 950°C depending on the reaction. The dehydration and decarbonation reactions require temperatures as high as 500 and 800°C. These elevated temperatures can be reached by special design of the solar collectors as mentioned by Cespedes et al (2014).

In the hydration of metal oxides, water vapor or humid air, as the working fluid, is used to realize the exothermic hydration reaction. The reverse endothermic

dehydration reaction uses either solar or waste heat to evaporate the chemically bound water from the metal oxide. The metal carbonates are also available for storing chemical heat where the working fluid is being carbon dioxide. For low temperature heat storage applications around 100 and 200°C, salt hydrates can be used. Similar to the metal oxide chemical heat storage units, the working fluid is humid air.

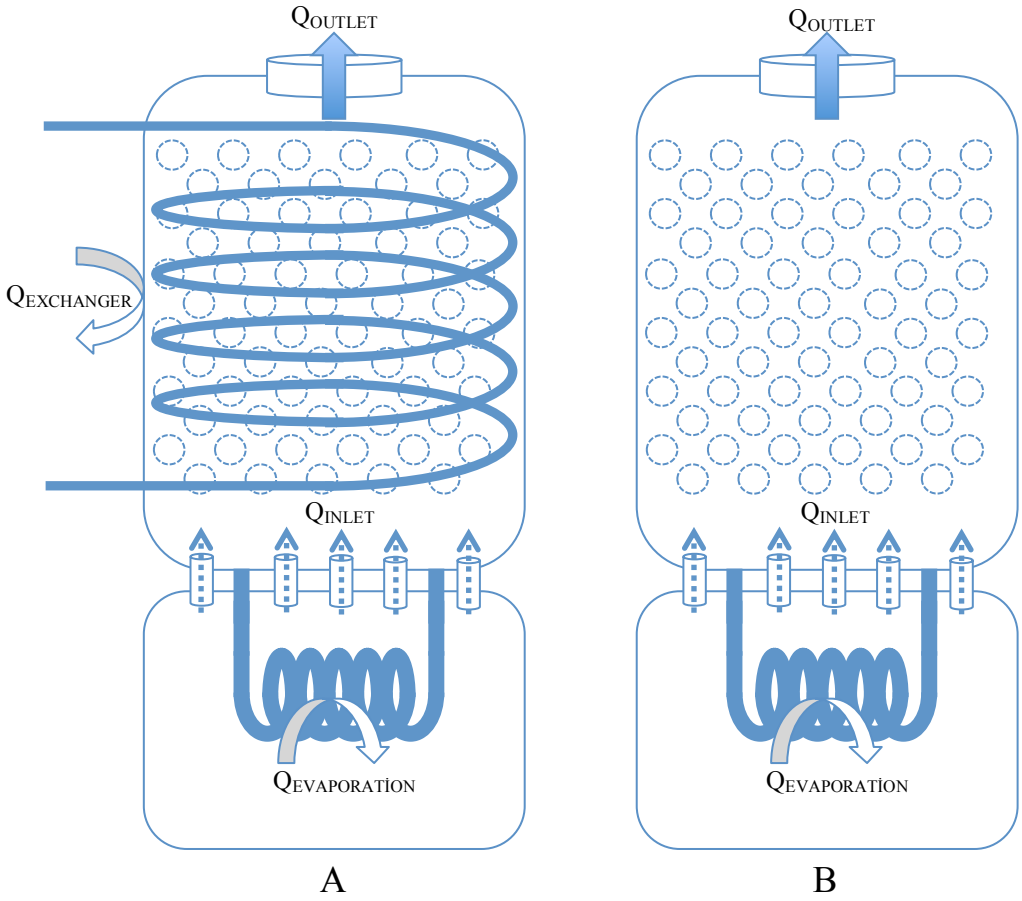

Figure 2.4. Scheme of direct and indirect concept in Thermochemical Energy Storage

There are two main thermochemical energy storage designs that are direct and indirect concept to store and release energy in a chemical energy storage. Depending on design, each system has various advantages and disadvantages compared to each other. Indirect concept is shown in Fig. 2.4(A), which illustrates water vapor flows within the reaction media, meanwhile heat transfer fluid flows into the pipe. This means heat transfer fluid is not contacted to CaO particles. This causes lower heat transfer performance. However in the direct concept a mixture of water vapor and

heat transfer fluid is supplied to the reaction media simultaneously. To put it in another way, heat transfer performance could be higher due to heat transfer fluid directly surrounding the particles. In contrast, this concept may have higher pressure drop.

2.2. Thermodynamics of hydration reactions for TCES cycles

In order to analyze thermodynamics of the reversible reactions to be used for TCES, let's represent the following table to give the standard enthalpies ΔH_f, and entropies S_f, of formation taking place in the reversible reactions.

Table 2.2. Standard enthalpy and entropy of formation for potential materials to be used for TCES.

Material	ΔH_f (kJ/mol)	S_f (J/mol K)
$H_2O_{(l)}$	-285.83	69.9
$H_2O_{(v)}$	-241.826	188.7
$CaO_{(s)}$	-634.92	39.88
$Ca(OH)_{2\,(s)}$	-986.1	83.4
$MgO_{(s)}$	-601.6	26.9
$Mg(OH)_2$	-924.5	63.2
$BaO_{(s)}$	-553.5	70.4
$Ba(OH)_{2\,(s)}$	-998.2	112

As it was represented in Figure 2.5, during the hydration reaction (charging step), the heat is released due to exothermic reaction. Contrary, in the charging step the endothermic dehydration reaction takes place in TCES unit and external energy such as solar energy or waste heat should be supplied. The dehydration reaction takes place at high temperatures. On the other hand, the hydration reaction occurs at low temperatures, as the Gibbs free energy is negative at lower temperatures. The thermodynamics of the reversible hydration/dehydration reaction for CaO will be explained in detail in section 3.1.

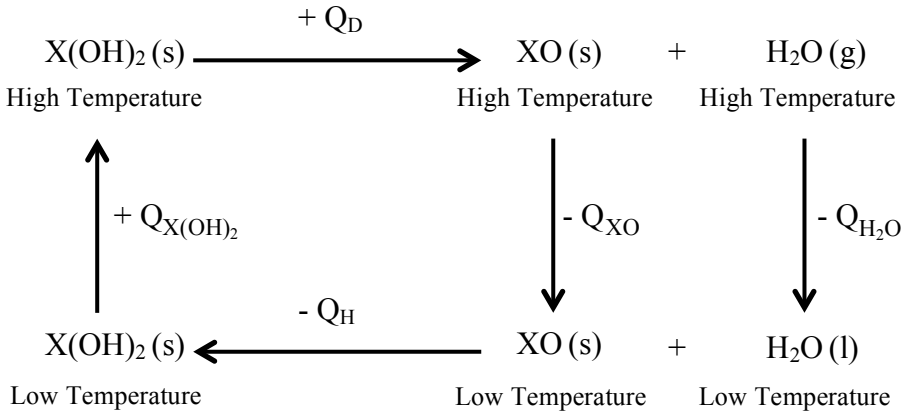

Figure 2.5. Diagram of the reversible reaction between hydration and dehydration.

In order to initiate the dehydration reaction, temperatures higher than the equilibrium temperature are required for the dehydration of the metal hydroxides. In Fig. 2.5, X may represent calcium or magnesium. Moreover, due to facility of the progress of the hydration reaction at low temperatures metal oxide releases heat and it can be easily stored at low temperatures. However if the water vapor is not stored at high temperatures, it also releases heat to the environment and energy loss from the system ($Q_{H2O.}$), occurs. Therefore, according to the nomenclature used in Figure 2.5, the heat loss of the system can be represented as;

$$Heat\ Lost\ Percentage = \frac{Q_{output}}{Q_{input}}.100 = \frac{Q_{XO} + Q_{H_2O}}{Q_D + Q_{X(OH)_2}}.100 \qquad (2.1)$$

The recovered heat can be defined as;

$$Q_{recovery} = Q_D + Q_{X(OH)_2} - \left(Q_{XO} + Q_{H_2O}\right) \qquad (2.2)$$

Actual stored heat can be calculated as;

$$Stored\ Energy\ Percentage = \frac{Q_{recovery}}{Q_{input}}.100 = \frac{Q_H}{Q_D + Q_{X(OH)_2}}.100 \qquad (2.3)$$

If water vapor produced in the dehydration step is supplied to the hydration reaction step at elevated temperatures, according to equation (2.2) Q_{H2O} term can be neglected and heat recovery would be higher.

$$Q_{recovery} = Q_D + Q_{X(OH)_2} - \left(Q_{XO} + Q_{H_2O}\right) \qquad Q_{H_2O} = 0 \tag{2.4}$$

In charging (storing) step, heat absorbed from an energy source as renewable (solar energy or waste energy) or conventional (fossil fuels etc.), is used for the dehydration of metal hydrates and salt hydrates or decarbonation of metal carbonates. The heat supplied for these reactions makes the endothermic reactions possible. As a result of dehydration and decarbonation reactions, the dehydrated salt and metal oxide or decarbonated metal oxide are produced.

Concerning the storing step, due to the dehydration and decarbonation reactions the heat can be stored without any or negligible heat loss. At the end of charging, the dehydrated metal oxide and waver vapor are at elevated temperatures as high as 510°C for CaO for example. It is not practical to try to keep the metal oxide at this temperature since there will be significant heat loss with time. Thus at the end of charging it is advantageous to extract heat from metal oxide and water vapor. This is also necessary to decrease the temperature as close to ambient temperature as possible for the storage of metal oxide and water vapor separately.

Due to the reversible reaction, in discharging step, water vapor is supplied to an anhydrous salt, anhydrous metal or carbon dioxide is supplied to metal carbonates. Thus a hydration or a carbonation reaction takes place in the storage unit. Because of this exothermic reaction, high thermal energy is released. Generally this process occurs at solar collectors. Thermo-chemical heat storage can be a correct choice for heating space or generating power considering the advantages such as recyclability, energy storage density, volume, expense and toxicity.

2.3. Advantages and disadvantages of chemical heat storage

The most important advantage of the TCES units is the highest energy density when it is compared to other type of thermal energy storages. Due to its high energy density, it requires less space for installing the heat storage unit. This is very important when the storage space is limited or valuable. In addition, the TCES systems facilitate keeping the chemical compounds separately at atmospheric conditions with no or negligible heat loss.

Table 2.3. Comparison of the three available technologies for seasonal thermal energy storage. (adapted from J. Xu et al., 2013)

	Sensible	Latent	Chemical
Storage Medium	-Water, gravel, pebble, soil.	-Organics, inorganics	-Metal chlorides, metal hydrides, metal oxides…
Type	-Water based system (Water tank, Aquifer) -Rock or ground based system	-Active storage -Passive storage	-Thermal-sorption (Adsorption, Absorption) -Chemical reaction (Normally for high-temperature storage)
Advantage	-Environmentally friendly cheap material -Relative simple system, easy to control -Reliable	-Higher energy density than sensible heat storage -Provide thermal energy at constant	-Highest energy density, compact system -Negligible heat losses
Disadvantage	-Low energy density, huge volumes required for district heating -Self discharge and heat losses problem -High cost of site construction -Geological requirements	-Lack of thermal stability -Crystallization -Corrosion -High cost of storage material	-Poor heat and mass transfer property under high density condition -Uncertain cyclability -High cost of storage material
Present status Future Work	-Large-scale demonstration plants -Optimization of control policy to advance the solar fraction and reduce the power consumption -Optimization of storage temperature to reduce heat losses -Simulation of ground/soil based system with the consideration of affecting factors (e.g. Underground water flow)	-Material characterization, laboratory-scale prototypes -Screening for better suited PCM materials with higher heat of fusion -Optimal study on store process and concept -Further thermodynamic and kinetic study, noble reaction cycle	-Material characterization, laboratory-scale prototypes -Optimization of the particle size and reaction bed structure to get constant heat output -Optimization of temperature level during charging/discharging process -Screening for more suitable and economical materials -Further thermodynamic and kinetic study, noble reaction cycle

Because of the low heat losses, the TCES systems are suitable for long term thermal energy storage applications. On the other hand, some of the TCES units have lower stability, relatively slow kinetics and corrosive effect.

The design and construction of the TCES systems are technically complex and require high initial investment. When the $CaO/Ca(OH)_2$ system is considered, the system has more advantages compared to its drawbacks. According to Pardo et al. (2014), it was underlined that TCES unit has high material energy density (experimental: 300 kWh/m^3). The system doesn't require catalyst, the reversibility of the reaction is high which is almost 22 cycles according to Schaube et al. (2012) and 100 cycles according to Pardo et al. (2014) depending on the design of the TCES system. As a conclusion for the reversible chemical reactions there is no by-product and, by the same token, products can be easily separated and stored.

Another important advantage of $CaO/Ca(OH)_2$ system is the operating pressure as 1 bar (Schaube 2012, 2013) Moreover the product can be easily found from ceramic or food industry etc., the price of product is low and finally no toxicity was reported.

The system has some drawbacks such as agglomeration and sintering of the material, the volume change of material and the low conductivity. Comparison of the TCES units is represented in Table 2.3. (J. Xu et al., 2013).

CHAPTER 3

MATHEMATICAL MODELING

In the following sections of this chapter, first the information concerning the thermodynamics and kinetics of hydration reaction will be presented. Following the sections on reaction thermodynamics and kinetics, the mathematical models will be explained to represent the operation of a TCES unit during the hydration (heat recovery) cycle.

The previous works done covered experiments performed for limited input parameters such as the inlet temperature and working fluid flow rate. Similarly the models representing the chemical heat storage unit for hydration/dehydration of CaO (Schaube et al., 2013, Fujimoto et al., 2002, Darkwa, 1998) were checked with the limited experimental data. Unfortunately there is no clearly defined model to be used for design and optimization in order to represent the input, output and state variables relations using the healthy reaction kinetics data.

3.1. Thermodynamics of CaO Hydration

The hydration/dehydration reaction of CaO is a reversible reaction. Thermodynamic data for the reaction were given in Table 3.1. These data will be used to compute the energy balance and the equilibrium temperature values.

Table 3.1. Enthalpy, Entropy and specific heat of water vapor and liquid, solid CaO and Ca(OH)

Material	ΔH_f (kJ/mol)	S_f (J/mol K)	Cp_{av} (J/mol K)
$H_2O_{(l)}$	-285.83	69.9	232
$H_2O_{(v)}$	-241.826	188.7	38.95
$CaO_{(s)}$	-634.92	39.88	49.95
$Ca(OH)_{2\,(s)}$	-986.1	83.4	19.0

Standard heat of reaction of CaO hydration at 25°C can be calculated as;

$$\Delta H = \Delta H_{f\,Ca(OH)_2} - \left(\Delta H_{f\,CaO_{(s)}} + \Delta H_{f\,H_2O_{(v)}} \right) \quad (3.1)$$

ΔH = -986.1 - (-634.92 -241.826) = -109.354 kJ/mol

Similarly the entropy change is ΔS = 83.4-(39.88+188.7)= -145.18 J/mol K. In these calculations the heat and entropy of formation of water vapor are used. The temperature range for the realization of this reaction can be calculated using the second law of thermodynamics. The Gibbs free energy change should be negative in order the reaction occur spontaneously (Çengel and Boles, 2012).

$$\Delta G = \Delta H - T.\Delta S < 0 \quad (3.2)$$

-109354+145.18 T<0 T<109354/145.18 K T<753.23K (480.1 °C)

Hydration reaction occurs at temperatures below 753.23 K. Temperatures above this value force the reaction to occur in the reverse direction which is the dehydration reaction. The hydration reaction gives an energy of 109.354 kJ/mol of CaO. The maximum temperature can be reached in the TCES using CaO/$Ca(OH)_2$ system, will be 480.1°C which is the above calculated thermodynamic equilibrium temperature. In the previous works (Abedin and Rosen , 2011, Schaube et al., 2012, Schmidt, 2013) concerning the dehydration of $Ca(OH)_2$, the temperature for the progress of the reaction was reported to be above 510°C at higher pressures.

The heat and entropy of formation of liquid water are used to calculate the heat of reaction and thus the temperatures at which the hydration and dehydration reactions can be obtained.

ΔH = -986.1 - (-634.92 -285.8) = -65.2 kJ/mol

The change in the heat capacities;

$$\Delta C_p = C_{p\ [Ca(OH)_2]} - (C_{p\ [CaO]} + C_{p\ [H_2O]}) . \quad (3.3)$$

ΔC_p = 87.5 - (46.0+104.9) = -63.4 J/mol.K

$$\Delta H(T) = \Delta H(T_R) + \Delta C_p (T - T_R) \qquad (3.4)$$

$$\Delta H = -65200 - 63.4 \times (510-25) = -95\,949 \text{ J/mol}.$$

The heat of dehydration reaction at 510°C was used to be 94.6 J/mol by Azpiazu et al. (2003). The thermodynamic data can be used to predict the equilibrium pressure of water vapor to make the hydration reaction progress. At equilibrium, the Gibbs free energy change can be written in terms the equilibrium constant $\Delta G = -RT\ln(K)$ where $K=P_v/P_o$. By doing the necessary mathematical manipulation

$$\ln\left(\frac{P_v}{P_o}\right) = -\frac{\Delta H}{RT} + \frac{\Delta S}{R} \qquad \ln\left(\frac{P_v}{P_0}\right) = -\frac{13.15}{T} + 17.47 \qquad (3.5)$$

This information will be used to calculate the necessary vapor pressure for the reaction to proceed to hydration and to include the effect of the vapor partial pressure on the reaction rate.

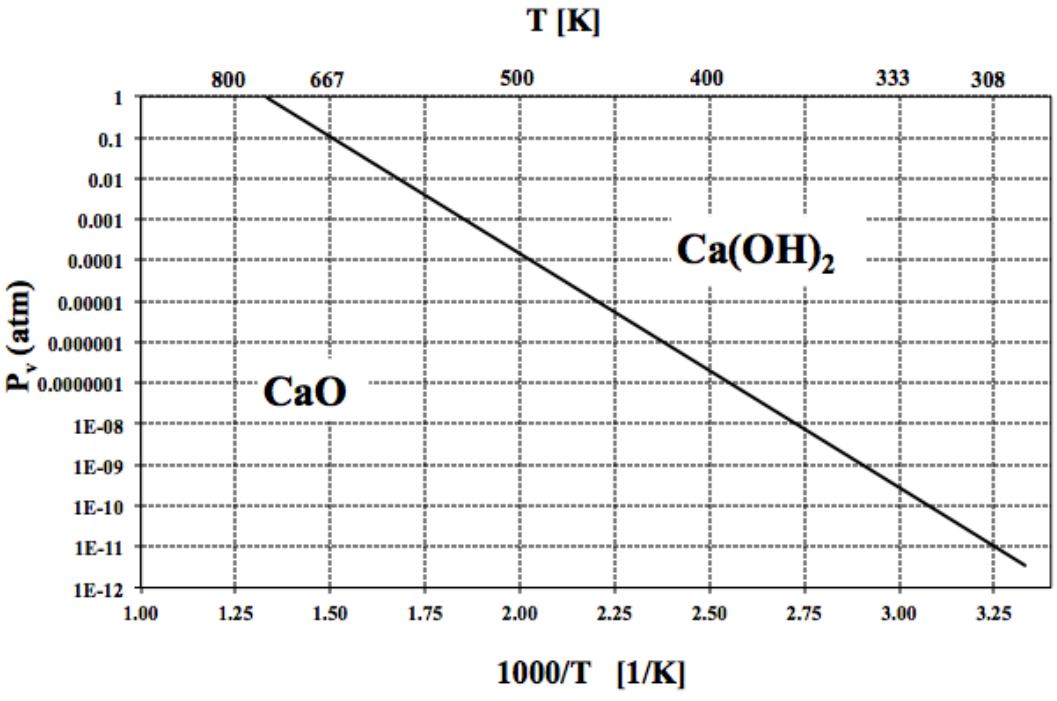

Figure 3.1. Thermodynamic equilibrium pressure as a function of temperature between 300 and 753 K and 1 atm total pressure.

The equilibrium temperature determined by thermodynamic calculations above indicates the hydration reaction takes place under 753.15 K. In order to realize hydration reaction in TCES unit, required minimum water vapor pressure was calculated by Van't Hoff equation (Eq. 3.5). The Fig. 3.1 shows the required water vapor pressure as a function of (1000/T). As it can be clearly understood from the results and Figure 3.1, water vapor pressure should be above the line if working temperature varies between 300-753K.

3.2. Reaction Kinetics of CaO Hydration

Dynamic simulation of $CaO/Ca(OH)_2$ chemical heat pump was modeled by Fujimoto et al. (2002) by considering the dehydration and hydration reactors two separate batch reactors. The hydration rate shown in equation (3.6) was considered to be a first order reaction with respect to the CaO mass fraction.

$$\frac{d\,C_{CaO}}{d\,t} = -k_h\,C_{CaO} \tag{3.6}$$

The effect vapor pressure was not taken into account in the kinetics equations. The hydration rate constant was given by the following equation

$$k_h = \frac{875\exp(-4.18\times10^4 / RT)}{1+51.1\exp(-1.096\times10^4 / RT)} \tag{3.7}$$

It was reported that the hydration rate equation of Fujimoto et al. (2002) was adopted from an experiment. Reaction rate of hydration increases during hydration process reported by Fujimoto et al. (2002). This is not an reasonable result when the equilibrium temperature (753K) of the hydration reaction of CaO is reached. Using the unsteady-state batch model equations for the chemical heat pump they computed the energy and exergy analysis around the heat pump. In the same work (2002) the differential equations were solved using the Euler's method. Fujimoto et al. worked for a low temperature range varying from around 10 to 30°C. The reactor dimension was given to be a length of 1.28 m and a diameter between 0.3 and 0.5 m.

The study of Shao et al. (2013) builds on a one-dimensional model and contributes better understanding of calcium oxide/calcium hydroxide energy system's

applications industrially. The system used by Shao et al. had a diameter of 0.055m and a length of 0.08 m. They investigated the impact of reaction rate, gas mass flux, porosity, and particle diameter.

According to Shao et al. (2013) the hydration reaction rate was reported as following equation;

$$\frac{d\,C_{CaO}}{d\,t} = -X_{mv}(\rho_{Ca(OH)} - \rho_{solid(CaO)})k_R^H \cdot \frac{T_s - T_{eq}}{Teq} \cdot \frac{C_{CaO}(t)}{C_{CaO(initial)}} \qquad (3.8)$$

In this equation ρ is density in kg/m^3, k_R^H is hydration reaction constant and X_{mv} is a factor that has to be added for the limitation of transport. In the work of Shao et al. k_R^H was varied depends on the slow and fast kinetics. According to the equation (3.8), equilibrium temperature of hydration reaction of CaO is taken into consideration.

It was reported in the Shao et al. (2013) that porosity change narrowed time of the reaction. On the contrary, porosity decrease caused lower permeability and thus increased equilibrium temperature. Moreover, particle diameter was also an important parameter on thermal behavior of charging/discharging process. It was concluded that slow heat transfer rate inhibits temperature difference between the solid and gas to increase.

The work of Schmidt et al.(2013), covered an experimental investigation of the dehydration and hydration reaction cycles using CaO/$Ca(OH)_2$ in a packed bed reactor. Air as HTF (Heat Transfer Fluid), and water vapor as the reactant, were fed separately into the system called indirect reactor. A reactor with a volume of 45 liters was designed for dehydration of the 20 kg of $Ca(OH)_2$. In their work, limitation for charging and discharging characteristic of the reactor has been studied experimentally owing to heat and mass transfer. The temperature profiles of inlet and outlet air stream in the reaction bed were observed in addition to the conversion rate during dehydration. The high temperature fluid is air and its flow rate varies between 0.00283 and 0.0531 kg/s. The maximum flow rate of the ambient is 160nm^3/hour for dehydration at 10 bar (0.0531 kg/s) and it was heated up around 700°C for dehydration by using electrical heaters. The conversion is defined as the ratio of the amount of water absorbed or released during the reaction to the theoretically

calculated stoichiometric amount of water as given by equation (3.9);

$$c[\%] = \frac{\Delta m\ [H_2O\ (\text{Heat Exchanger})]}{\Delta m\ [H_2O\ (\text{Stoichiometric})]} \tag{3.9}$$

Theoretical amount of water was calculated to be m [H_2O (Stoichiometric)]=4.871kg. When the hydration cycle was completed, the overall conversion was measured to be 76.5% according to the experiments performed.

The equilibrium relation was owing to Samms and Evans data at 510°C, at a vapor pressure of 1 bar that can be represented as;

$$\ln\left(\frac{P_{H_2O}}{[bar]}\right) = -\frac{11.375}{T[K]} + 14.547 \tag{3.10}$$

During the whole process the water vapor pressure was determined around 1.985 bar experimentally and kept constant at around that value. By means of using the equation (3.10), an equilibrium temperature was calculated to be around 546°C. The reaction temperatures at different locations within the bed were recorded by thermocouples. It was observed that thermocouples placed at half way and close to the reactor exit reached a maximum reaction temperature between 542 to 549°C. These results were reported to be in good agreement with the values reported by Samms and Evans equation given by Eq. (3.10)

In the work of Schaube et. al. (2012), the enthalpy change of dehydration reaction was studied. For the determination of equilibrium in terms of temperature and pressure, Samms and Evans data, Halstead and Moore data and Matsuda were compared. There was no reported difference between their data in contrast to Schaube data and Matsuda's data. The difference between those data was due to experimental conditions. And the equilibrium equation was represented as;

$$\ln\left(\frac{P_{eq}}{10^5}\right) = -\frac{12.845}{T_{eq}} + 16.508 \tag{3.11}$$

Therefore according to equation (3.11), the temperature of 505°C can be reached when the H_2O partial pressure is 1 bar. In Schaube et al.'s paper (2012), the effect of

the heating rate on the onset temperatures (temperatures at which the dehydration is initiated) was determined by using equilibrium temperatures. In the same way due to the Van't Hoff equation , the reaction enthalpy can be determined as;

$$\ln P_{eq} = -\frac{\Delta H}{RT_{eq}} + const. \tag{3.12}$$

As a result of this equation, ΔH varied to be 94.6 kJ/mol, 104.3 kJ/mol or 106.8 kJ/mol according to the works of Samms and Evans, Halstead and Moore and the Schaube et al., respectively. The measurements in the work of Schaube et al. were performed using differential scanning calorimetry for which a constant signal could not be obtained before and after the dehydration. In order to overcome that situation the sample was cooled down and for initiating the rehydration, water vapor was released to the working fluid atmosphere. Using the mass change data, enthalpy of the reaction was determined to be ΔH =111.8 kJ/mol. However, the DSC results showed that the reaction enthalpy varied from 94.6 to 111.8 kJ/mol.

For better understanding of conversion behavior under different experimental conditions, de- and re-hydration cycles had been investigated by Schaube et al. (2012, 2013). At the end of 100 cycles, it was observed that the rehydration had taken place at 452°C and 95.6 kPa because of the possible changes in the solid structure of CaO.

The reaction rate constant was given by the Arrhenius law and it was expressed as;

$$K(T) = A.\exp\left(\frac{-E}{RT}\right) \tag{3.13}$$

where A defines the pre-exponential factor and E the activation energy. The dehydration rate kinetics relations were represented by the following relation in order to include the effect of the pressure and experimental results were reported to give satisfactory agreement with the proposed rate expressions given as equation (3.14).

$$\ln\frac{dX}{dt} = \ln A - \frac{E}{RT} + \ln f(X) + \ln h(P, P_{eq}(T)) \tag{3.14}$$

In the same work of Schaube et al. (2012), Arrhenius law and pressure terms were taken into consideration. Activation energy of 89.486± 0.91 and pre-exponential factor of 1.394×10^4 were reported for hydration reaction. Therefore overall equation for hydration reaction was expressed as;

For $T_{eq} - T \geq 50K$,

$$\frac{dX}{dt} = 13945.\exp\left(\frac{-89.486\times10^3}{RT}\right)\left(\frac{P}{P_{eq}}-1\right)^{0.83}.3(1-X).\left[-\ln(1-X)\right]^{0.666} \qquad (3.15)$$

and for $T_{eq} - T < 50K$ and $P > P_{eq,}$

$$\frac{dX}{dt} = -1.0004\times10^{34}.\exp\left(\frac{53.332\times10^3}{T}\right)\left(\frac{P}{10^5}\right)^5.(1-X) \qquad (3.16)$$

In the work of Schaube et. al. (2013a) the heat transfer characteristics were searched due to fast heat transfer in and out of the reactor. The reaction rate was defined as a function of the temperature distribution. The gaseous H_2O and nitrogen were supplied to reaction media. This concept is known as direct operation. In the direct operation of the TCES unit, the HTF was also used as transportation medium for the gaseous reactant and system doesn't require external heaters. Higher heat transfer rates and higher power levels can be obtained using the direct operation. In the direct concept, the heat transfer fluid was forced to flow through the bed in order to enhance the heat transfer and obtain high power levels. Experimental set up was designed and experiments were conducted to examine primarily the characteristics of direct heat transfer. It was considered that the heat was not only transferred to the ambient but also due to the fluid flowing through the reactor. The process was limited by the reaction rate rather than the heat transfer rate.

In the work of Ogura et. al.(1999), the heat generation in chemical heat pump using the reaction between calcium oxide and calcium hydroxide, was studied both experimentally and theoretically. For investigating the reversible chemical reaction, they solved the model equations for three different cases such as negligible fluid velocity and diffusion, negligible fluid velocity and negligible diffusion only. The computations were performed to simulate the cold/hot heat generation cycles of chemical heat pump.

The reaction rate of single CaO particle was given by the following equation; (which was reported by Matsuda et. al. 1985).

$$\frac{dX}{dt} = k(1-X)^{2/3}.(P_W - P_P) \qquad (3.17)$$

In this equation, P_P and P_W refers to reaction equilibrium pressure of $CaO/Ca(OH)_2$ particle and saturated vapor pressure calculated from water temperature in evaporator, respectively. The calcium oxide was prepared by de-carbonation of CaCO (limestone) at about 1223K in electrically heated furnace. The purity of the $CaCO_3$ was reported to be 99% and the particle diameter range was 710-1000 μm. In the model, the effects of both the diameter and vertical length on the state variables were taken into account. The conversion and temperature profiles for radial and vertical direction were obtained. They compared the model and experimental results and reported that a good agreement was obtained.

In the work of Ogura et. al. (2001, 2002) chemical heat pump dryer using the hydration/dehydration reaction of CaO to $Ca(OH)_2$, was studied experimentally. The heat pump of Ogura et al. (2002) was consisted of two separate reactors with diameters of 60 mm and 288 mm. The energy required for drying was supplied by the hydration of CaO reaction. In the experiments, the overall conversion and temperature profiles were obtained for two different cases using 4.8 kg CaO and 6.0 kg CaO. They repeated the experiments for different air flow rates and initial conditions. One important observation of the experimental results in question was that the hydration reaction occurred almost instantaneously showing a maximum temperature rise between 500 and 550K for an air flow rate of 38 L/min depending on the location of the thermocouples. The air flow rate was kept at 38 and 43 L/min and it was observed that the maximum temperature reached decreased to around 450K at 43 L/min due to the heat removed by the flowing air. They compared the energy efficiency of the hydration reactions under different conditions but they could not come out with an abstract conclusion, as the energy efficiencies did not make a comparison based on the working fluid flow rates.

Zamengo et al. (2014) investigated the hydration and dehydration of MgO using a closed system. In the work of Zamengo et al. (2014), thermochemical performance of

magnesium hydroxide-graphite pellets were experimentally studied for the chemical heat pump. The packed bed pellets were settled in the middle of the reactor chamber. The thermocouples placed in reaction chamber to determine the temperature change. The heater surrounded the reaction chamber. The reaction chamber was weighed to investigate the water vapor consumption rate. Fig 3.2 illustrates the semi batch packed bed chemical energy storage system of Zamengo et al. (2014).

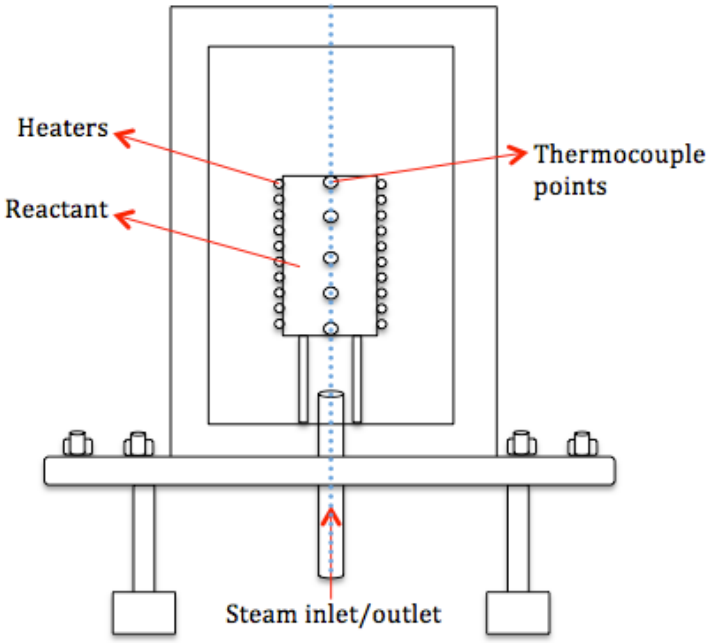

Figure 3.2. The schematic representation of the semi batch packed bed chemical heat storage unit (adapted from Zamengo et al. (2014)).

According to the system of Zamengo et al. (2014) is shown in Fig 3.2, in the dehydration step, inside of the reactor, temperature was set at 400°C using an external heater. The water vapor released by chemical reaction was collected in a water reservoir. In the hydration step, the reaction media was cooled down to 120°C. Thus the water reservoir was kept to store water vapor at 100°C. When the reaction was started , the valve, situated between reaction media and water reservoir, was opened and the hydration reaction started in the reaction chamber. As it is clearly understood from their experiments, it is a semi batch system due to inlet and outlet steams during the hydration and dehydration reactions. Because there is no outlet flow when the hydration occurs. On the other hand there is no inlet flow as the dehydration reaction is present.

3.3. Heat transfer phenomena during the hydration of CaO in a packed bed

There are three main mechanisms of heat transfer occurring in a packed bed of CaO reacting with water vapor to give $Ca(OH)_2$. These are conduction, convection and radiation.

- Conduction occurs between the solid reactant particles.
- Depending on the design of the heat storage unit, there may be two different aspects of convective heat transfer. These are the convection between the solid reactant and working fluid in addition to the convective heat transfer between the solid reactant and indirect heating fluid such as air for indirect heating purpose. The heat loss through the walls of the heat storage unit may occur due to convection.
- Radiative heat transfer may occur similar to the convective heat transfer between the solid reactant and the working fluid. Same as above, the heat loss due to radiation may occur through the walls of the heat storage unit.

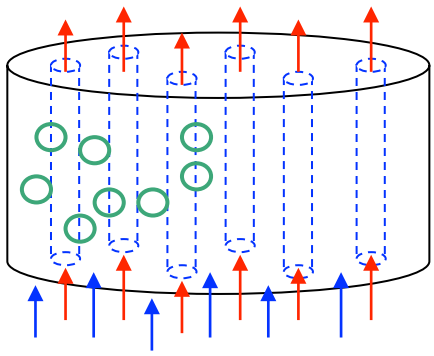

Figure 3.3. Schematic representation of TCES unit using air for indirect heating.

In a TCES, three modes of heat transfer phenomena namely conduction, convection and radiation define the thermal behavior of the system investigated. The convective heat transfer phenomenon can also be from the inner wall of the reactor to the surrounding. The convective heat transfer rate can be represented using the Newton's law of cooling;

$$\frac{Q}{A_C} = h\,(T_f - T_S) \qquad (3.18)$$

where the rate of convective heat transfer is Q. in W (J/s) from the gas at T_f in °C to surface of the solid at T_s in °C, and A_c is the surface area in m^2.

Heat transfer by conduction can also be present simultaneously with convection in a TCES. The conductive heat transfer occurs between the solid particles and through the walls of the TCES as well. The differential form of the overall heat transfer rate due to conductive heat transfer is represented using the Fourier's law of heat conduction given by equation (3.19).

$$\frac{Q}{A_C} = -k\frac{dT}{dx} \tag{3.19}$$

where Q is rate of conduction between the solid particles and *k* is the conductive heat transfer coefficient.

In addition to all, the radiant heat transfer can also take place between the working fluid and solid particles. The radiant heat transfer is defined as follows; where ε is the total emissivity of surface, σ is the Stefan Boltzmann constant which is 5.676 x 10^{-8} W/m^2K^4, T_1 and T_2 are the temperatures of the hot and cold surfaces, respectively.

$$\frac{Q}{A_C} = \varepsilon\sigma\,(T_1^4 - T_2^4) \tag{3.20}$$

A research to investigate thermal efficiency and charging / discharging behavior for a packed be thermal storage by means of numerical model and experiment results was discussed by Hanchen et. al. (2011)

Hanchen et al. (2011) put forward the view that the sensible heat storage using air as HTF in a packed bed of rocks could be proper considering high temperature storage. Work of Hanchen et al. (2011) reported that system has no required equipment and limitations on operating parameters such as temperature and pressure. In order to increase the reliability of the model, model was tested for the parameters of a previous work. In the work of Hanchen et al. (2011), results were obtained for different time periods (persistent 6-h charging 6-h discharging daily and same charging/discharging period for one time). As a result, Hanchen et al. (2011) observed the overall efficiency reached to be above 90%. On the basis of the results, it seems fair to suggest that material should have high volumetric heat capacity and

small particle size with low air flow rate for obtaining high overall efficiency

The work of Mawire et al. (2009) is an attempt to address the issue of thermal performance of different storage materials for a system of oil-pebble bed thermal energy storage. They analyzed the thermal performance of a pebble bed for sensible heat storage by using one-dimensional model. Silica glass, alumina and stainless steel were used as storage material. In general, air, water or oil as a heat transfer fluid can be used in pebble beds for sensible heat storage. In the work of Mawire et al., oil was used as a HTF because of high operating temperature range. In the model of Mawire et al., pebble bed was designed at 0.29 m in diameter and 0.30 m in height with a void fraction of 0.42. Temperature distributions were simulated for three different materials that are silica glass, alumina and stainless steel. Simulation results were compared with a previous work of Mawire et al. in 2005. Five thermocouples were located at different points with 30 cm of distances between bottom and top. Temperature at center of the bed showed the largest difference between experiment and simulation. Due to the higher conductivity of alumina, it performed larger temperature difference. Therefore alumina showed the fastest energy storing performance compared to other materials. On the contrary, fused silica showed the highest temperature difference in consequence of low thermal conductivity of silica. Total energy storing profile, total exergy storing profile and ratio of total exergy to total energy were also computed for three different storage materials. In this case, stainless steel gave the best result related to total energy stored. Whereas stainless steel showed a rapid increase and highest decrease on total energy storing. Thus, an optimal charging time was required due to a huge decrease. Moreover, stainless steel also showed the best performance on the total exergy storing. Furthermore alumina gave the best result concerning to ratio of total exergy to total energy.

3.4. Lumped and Distributed Parameter Models

The modeling of TCES unit can be done in several ways depending on the complexity of the model. In the present thesis two different approaches will be presented such as lumped and distributed parameter models.

Lumped parameter model: State variables are considered to be a function of time only. In other words variables such as temperature and concentration were used as

average values for the whole system. Model equations will be ordinary differential equations and numerical solution techniques such as Euler's methods can be used.

Distributed parameter model: State variables are considered to be a function of the geometry of the TCES unit in addition to time. Model equations will be partial differential equations representing the differential changes with respect to the axial position and time.

As it will be explained in detail in Chapter 5 Results and Discussion, the results of the LPM will give a general idea on the limitations of the hydration reaction, the heat release rate and the effect of the water vapor flow rate for a given mass of calcium oxide to satisfy a certain heat requirement. Complementary to the LPM, the DPM will also answer the possible alternatives to adjust the water vapor supply and heat removal profiles for a predefined dimension of the heat storage unit such as diameter, height and mass of the calcium oxide. Briefly, the results of the LPM and DPM together will help us to develop alternative conceptual designs and for understanding and analyzing the ranges of the parameters to be used in the conceptual design of a thermo-chemical energy storage unit.

There has been relatively little literature on TCES systems and a commercial design has not been enhanced yet. Numerous experiment studies separates into two different systems, which are open and closed systems concerning the related works own design. In a closed system, thermal behavior of heat storage by using reaction between CaO or MgO and water vapor, were analyzed for different variables such as; temperature and weight in the work of Darkwa et al. (2006), and Zamengo et al. (2014).

Moreover water vapor and nitrogen mixture was supplied as a HTF fluid in the open system and temperature at different point in addition to outlet temperature of the fluid were measured by Schaube et al. (2013).

With the inspiration by the works mentioned above, model equations will be solved and explained individually for closed system as LPM and for open system as DPM.

3.4.1. Lumped Parameter Model

In the lumped parameter model state variables such as the fluid and solid temperatures, concentrations of reactants are considered to be a function of time only. The following assumptions are made while developing the differential model equations for lumped parameter model:

- Constant thermal and physical and thermal properties of the solid and working fluid.
- Temperature gradients in axial and radial directions, in other words, the effect of the conductive heat transfer in axial and radial directions are negligible.
- Heat transfer due to radiation is negligible.
- Heat transfer between the working fluid and solid occurs only due to convection.
- Heat loss is negligible.
- There is no resistance to mass transfer at the solid surface. This is to say the rate of transfer of water vapor is not the limiting step of the reaction rate.
- Void fraction and porosity are constant.
- There is no temperature gradient within the solid particles.

Here a simplified model giving the governing unsteady state energy conservation equations will be presented. The differential mass and energy balances for the gas and solid phases will be written separately.

$$\begin{bmatrix}\text{Energy flowing}\\ \text{into the TCES with}\\ \text{working fluid during}\\ \Delta t \text{ period}\end{bmatrix} - \begin{bmatrix}\text{Energy flowing}\\ \text{out of the TCES with}\\ \text{working fluidduring}\\ \Delta t \text{ period}\end{bmatrix} + \begin{bmatrix}\text{Energy content of}\\ \text{the fluid at time t}\\ \text{within the TCES}\end{bmatrix} - \begin{bmatrix}\text{Energy content of}\\ \text{the fluid at time t}+\Delta t\\ \text{within the TCES}\end{bmatrix}$$

$$- \begin{bmatrix}\text{Energy transferred by convection}\\ \text{between the solid particles}\\ \text{and working fluid during } \Delta t \text{ period}\end{bmatrix} = 0$$

$$\rho_f C_{p_f} v \varepsilon A_c T_{f_{in}} \Delta t - \rho_f C_{p_f} v \varepsilon A_c T_f(t) \Delta t + \rho_f C_{p_f} T_f(t) \varepsilon A_c L$$

$$- \rho_f C_{p_f} T_f(t+\Delta t) \varepsilon A_c L - h a A_c L (T_f(t) - T(t)) \Delta t = 0 \quad (3.21)$$

After dividing the above equation by $A_c \times \Delta t$ and taking limit as Δt approaches zero, the differential energy balance for the fluid phase becomes;

$$\rho C_p \varepsilon L \frac{dT_f}{dt} = \rho_f C_{p_f} v \varepsilon T_{f_{in}} - \rho_f C_{p_f} v \varepsilon T_f - h a L \left(T_f - T \right) \quad (3.22\text{ a})$$

During the hydration of CaO, the water vapor flow rate is the limiting or rate controlling parameter. Thus in the packed bed of chemical heat storage unit, the heat flow out of the system at the fluid temperature does not exist for closed system design. That is to say the fluid phase differential energy balance for the closed system is given as follows;

$$\rho C_p \varepsilon L \frac{dT_f}{dt} = \rho_f C_{p_f} v \varepsilon T_{f_{in}} - h a L \left(T_f - T \right) \quad (3.22\text{ b})$$

Similarly the differential energy balance for the solid phase is given as follows;

$$\begin{bmatrix} \text{Energy content of} \\ \text{the solid at time t} \\ \text{within the TCES} \end{bmatrix} - \begin{bmatrix} \text{Energy content of} \\ \text{the solid at time t+}\Delta\text{t} \\ \text{within the TCES} \end{bmatrix} - \begin{bmatrix} \text{Energy transferred by convection} \\ \text{between the solid particles} \\ \text{and working fluid during } \Delta\text{t period} \end{bmatrix}$$

$$+ \begin{bmatrix} \text{Energy released by chemical} \\ \text{reaction within the solid particles} \\ \text{during } \Delta\text{t period} \end{bmatrix} = 0$$

$$\rho_s C_{p_s} T(t)(1-\varepsilon) A_c L - \rho_s C_{p_s} T(t+\Delta t)(1-\varepsilon) A_c L$$

$$- h a A_c L (T(t) - T_f(t)) \Delta t - \frac{dC_{CaO}}{dt} \Delta H_r (1-\varepsilon) A_c L \Delta t = 0 \quad (3.23)$$

In the above equation after dividing all terms by $A_c \times L \times \Delta t$ and taking limit as Δt approaches zero the following equation is obtained;

$$\rho_s C_{p_s}(1-\varepsilon)\frac{dT}{dt} = ha\left(T_f - T\right) - \frac{dC_{CaO}}{dt}\Delta H_r(1-\varepsilon) \tag{3.24}$$

As the reaction kinetics in section 3.2 was explained, here it will briefly be presented as the works of Fujimoto et al. (2002) and Shao et al(2013).

$$\frac{dC_{CaO}}{dt} = -k_h C_{CaO} \tag{3.6}$$

The hydration rate constant of Fujimoto et al. (2002) was given by the following equation:

$$k_h = \frac{875\exp(-4.18\times10^4 / RT)}{1+51.1\exp(-1.096\times10^4 / RT)} \tag{3.7}$$

The hydration rate equation of Shao et al (2013) was represented by following equation:

$$\frac{dC_{CaO}}{dt} = -X_{mv}(\rho_{Ca(OH)} - \rho_{solid(CaO)})k_R^H \cdot \frac{T - T_{eq}}{T_{eq}} \cdot \frac{C_{CaO}(t)}{C_{CaO(initial)}} \tag{3.8}$$

In the simulations, the above rate equation was used as it considers the effect of the thermodynamic equilibrium temperature on the reaction rate.

3.4.2. Distributed Parameter Model

Distributed parameter model considers the variation of the state variables with time and location within the packed bed. Therefore the developed model equations will be partial differential equations representing the variation of the state variables with respect to time and location. Thus the following assumptions are used while writing the model equations for the distributed parameter model.

- Temperature gradient in the radial direction is neglected.
- Constant thermal and physical properties of the solid and working fluid.
- Heat transfer due to radiation is negligible.
- Heat transfer between the working fluid and solid occurs only due to convection.

- Heat loss is negligible.
- There is no resistance to mass transfer at the solid surface. This is to say the rate of transfer of water vapor is not the limiting step of the reaction rate.
- Fluid velocity is constant across the radial direction (plug flow assumption).
- Void fraction and porosity are constant.
- There is no temperature gradient within the solid particles.

$$\begin{bmatrix}\text{Energy flowing}\\ \text{into the TCES with}\\ \text{working fluid at z}\\ \text{during } \Delta t \text{ period}\end{bmatrix} - \begin{bmatrix}\text{Energy flowing}\\ \text{out of the TCES with}\\ \text{working fluid at z+}\Delta z\\ \text{during } \Delta t \text{ period}\end{bmatrix} + \begin{bmatrix}\text{Energy content of}\\ \text{the fluid at time t}\\ \text{within the differential}\\ \text{control volume of TCES}\end{bmatrix}$$

$$- \begin{bmatrix}\text{Energy content of}\\ \text{the fluid at time t+}\Delta t\\ \text{within the differential}\\ \text{control volume of TCES}\end{bmatrix} - \begin{bmatrix}\text{Energy transferred by convection}\\ \text{between the solid particles and}\\ \text{working fluid within the differential}\\ \text{control volume of TCES}\end{bmatrix} = 0$$

Dividing the above differential energy balance by $A_c \times \Delta z \times \Delta t$ and taking limits as Δz and Δt approach zero, gives the following differential energy balance equation for the fluid phase.

$$\rho_f C_{p_f} \varepsilon \frac{\partial T_f}{\partial t} = \rho_f C_{p_f} v \varepsilon \frac{\partial T_f}{\partial z} - h a \left(T_f - T\right) \tag{3.25}$$

As the water vapor flows upward along the packed bed of CaO pellets, the hydration reaction occurs. Thus, temperature and CaO concentration profiles change with time and location along the packed bed heat storage unit. This will require the computations of the water vapor flow rate and the rate of heat removal from the system by taking into account the variation with height and time. Water vapor mass balance along the TCES unit can be expressed as equation as follows,

$$\frac{\partial \dot{m}_{H_2O}}{\partial z} = \frac{\partial C_{CaO}}{\partial t} .(1-\varepsilon).A_C.M_{W(H_2O)} \cdot \frac{1}{\varepsilon} \tag{3.26}$$

$$\begin{bmatrix}\text{Energy content of}\\ \text{the solid at time t}\\ \text{within the differential}\\ \text{control volume of TCES}\end{bmatrix} - \begin{bmatrix}\text{Energy content of}\\ \text{the solid at time t+}\Delta\text{t}\\ \text{within the differential}\\ \text{control volume of TCES}\end{bmatrix}$$

$$+ \begin{bmatrix}\text{Energy transferred by}\\ \text{conduction between the solid}\\ \text{particles within the differential}\\ \text{control volume of TCES at z}\end{bmatrix} - \begin{bmatrix}\text{Energy transferred by}\\ \text{conduction between the solid}\\ \text{particles within the differential}\\ \text{control volume of TCES at z+}\Delta z\end{bmatrix}$$

$$+ \begin{bmatrix}\text{Energy transferred by convection}\\ \text{between the solid particles}\\ \text{and working fluid within the differential}\\ \text{control volume of TCES}\end{bmatrix} - \begin{bmatrix}\text{Energy released by chemical}\\ \text{reaction within the differential}\\ \text{control volume of TCES}\end{bmatrix} = 0$$

So the differential energy balance around the heat storage unit for the solid phase can be written as follows,

$$\rho_s C_{p_s}(1-\varepsilon)\frac{\partial T}{\partial t} = k\frac{\partial^2 T_S}{\partial z^2} + ha\left(T_f - T\right) - \frac{\partial C_{CaO}}{\partial t}\Delta H_r(1-\varepsilon) \qquad (3.27)$$

The hydration rate equations will be the same as equation (3.8).

CHAPTER 4

NUMERICAL METHODS

Lumped parameter model is formed of ordinary differential equations representing the differential change of state variables with respect to time. Their solutions are realized using Euler's method. Distributed parameter model is defined using partial differential equations. The DPM equations represent the differential changes in state variables with respect to time and axial position. Their solutions are done using the finite difference method. In the following sections both methods will be explained.

4.1. Euler Method

Euler's method is the most basic solution technique of ordinary differential equations when initial-value problems are to be considered.

$$\frac{dy}{dz} = f'(x,y) \qquad y_{i+1} = y_i + f'(x,y).h \qquad y_{i+1} = y_i + \frac{dy}{dz}.h \tag{4.1}$$

$$\text{New Value} = \text{Previous Value} + \text{Slope} \,.\, \text{Step}$$

The main goal of Euler's method is to obtain approximations. Euler's method is used for ordinary differential equations with the slope of the function. For the solution of Euler's method, an initial value is required. Basic idea of Euler's method is estimation of the value of function at new step using the rate of change of the variable and the value of the variable know at the previous step. Preferably the rate of change or slope is only calculated for small intervals. Therefore, computation points follow each other consecutively.

The solid temperature, fluid temperature and CaO concentration at certain times between time t and t+Δt is shown in Fig. 4.1. These variables were calculated after being written in the following forms, equations (4.2)-(4.6), based on the Euler's method.

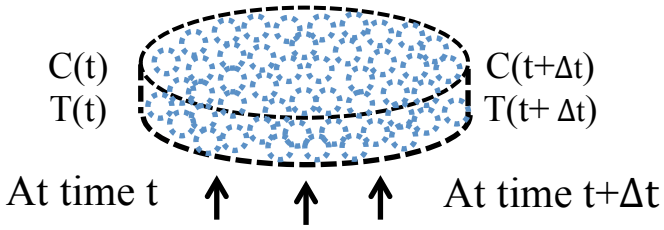

Figure 4.1. Schematic representation of temperature and concentration change.

The solid temperature was computed by simultaneously using equations (4.2), (4.3).

$$T(t+\Delta t) = T(t) + \frac{dT(t)}{dt}.\Delta t \tag{4.2}$$

where temperature change for time wise was desired;

$$\frac{dT(t)}{dt} = \underbrace{\left(\frac{h_{conv}.a.\left(T_f(t) - T(t)\right)}{\rho_f C_{p_f} \varepsilon} \right)}_{Fluid\,Convection} + \underbrace{\frac{dC_{CaO}(t)}{dt} \frac{\Delta H_r}{\rho_S C_{p_S}}}_{Reaction} \tag{4.3}$$

Similarly, temperature of the working fluid was determined as follows;

$$T_f(t+\Delta t) = T_f(t) + \frac{dT_f(t)}{dt}.\Delta t \tag{4.4}$$

where rate of change of temperature of the fluid was determined using;

$$\frac{dT_f(t)}{dt} = \underbrace{\left(\frac{-h_{conv}.a.\left(T_f(t) - T(t)\right)}{\rho_f C_{p_f} \varepsilon} \right)}_{Fluid\,Convection} + \underbrace{\left(\frac{\nu T_{f_{in}}}{L} \right)}_{Inlet\,Heat\,Transfer} \tag{4.5}$$

Calcium oxide concentration was determined using following equation;

$$C_{CaO}(t+\Delta t) = C_{CaO}(t) + \frac{dC_{CaO}(t)}{dt}.\Delta t \tag{4.6}$$

For determining calcium oxide concentration at each time, temperature change as a function of time was computed to test using the rate equations of Shao et al. (2013) and Fujimoto et al. (2002). These equations were explained in previous section (3.2).

According to Fujimoto et al. (2002), rate equation of hydration reaction can be expressed as;

$$\frac{dC_{CaO}}{dt} = -k_h C_{CaO} \tag{3.6}$$

where the rate constant of hydration reaction of calcium oxide is

$$k_h = \frac{875\exp(-4.18\times10^4 / RT)}{1+51.1\exp(-1.096\times10^4 / RT)} \tag{3.7}$$

According to Shao et al. (2013), rate equation of hydration of calcium oxide can be shown as;

$$\frac{dC_{CaO}}{dt} = -X_{mv}(\rho_{Ca(OH)} - \rho_{solid(CaO)})k_R^H \cdot \frac{T-T_{eq}}{T_{eq}} \cdot \frac{C_{CaO}(t)}{C_{CaO(initial)}} \tag{3.8}$$

Required water vapor flow rate equation as a function time only solved by equation as follows;

$$\dot{m}_{H_2O}(t) = \frac{dC_{CaO}}{dt} \cdot \frac{(1-\varepsilon)}{\varepsilon} \cdot A_C L M_{W(H_2O)} \tag{4.7}$$

This equations expresses that water vapor was supplied to the system as a function of the reaction rate. This is a closed system and thus all water vapor is used up in the TCES unit. The initial values used the solve the model equations were explained in detail in section 4.3.

4.2. Finite Difference Method

Finite difference methods are numerical techniques for the solution of partial differential equations. It is used when the analytical solutions are not possible due to non-linear terms and changing boundary conditions. In the finite difference method, derivatives of functions are replaced with approximations by differences (time and space discretized forms) in the values of the function for the independent variables. If x is the given value of independent variable with a small increment (x+Δx), then this method can be done by taking a Taylor expansion of function and Taylor series expansion of f can be written as follows,

$$f(x+\Delta x)=f(x)+(\Delta x)\frac{\partial f}{\partial x}+\frac{\Delta x^{2}}{2!}\frac{\partial^{2} f}{\partial x^{2}}+\frac{\Delta x^{3}}{3!}\frac{\partial^{3} f}{\partial x^{3}}+\ldots$$

$$=f(x)+\sum_{n=1}^{\infty}\frac{(\Delta x)^{n}}{n!}\frac{\partial^{n} f}{\partial x^{n}} \tag{4.8}$$

When taking the derivative of the function, the value of df/dx can be approximated a by using the finite difference approximation for (f(x+Δx)-f(x))/ Δx.

The approximation as;

$$\frac{\partial f}{\partial x}=\frac{f(x+\Delta x)-f(x)}{\Delta x}-\frac{(\Delta x)^{2}}{2!}\frac{\partial^{2} f}{\partial x^{2}}-\frac{(\Delta x)^{3}}{3!}\frac{\partial^{3} f}{\partial x^{3}}-\ldots \tag{4.9}$$

or with an error as follow,

$$O(\Delta x)=-\frac{(\Delta x)^{2}}{2!}\frac{\partial^{2} f}{\partial x^{2}}-\frac{(\Delta x)^{3}}{3!}\frac{\partial^{3} f}{\partial x^{3}}-\ldots \tag{4.10}$$

when the error to be considered it can be ,

$$\frac{\partial f}{\partial x}=\frac{f(x+\Delta x)-f(x)}{\Delta x}+O(\Delta x) \tag{4.11}$$

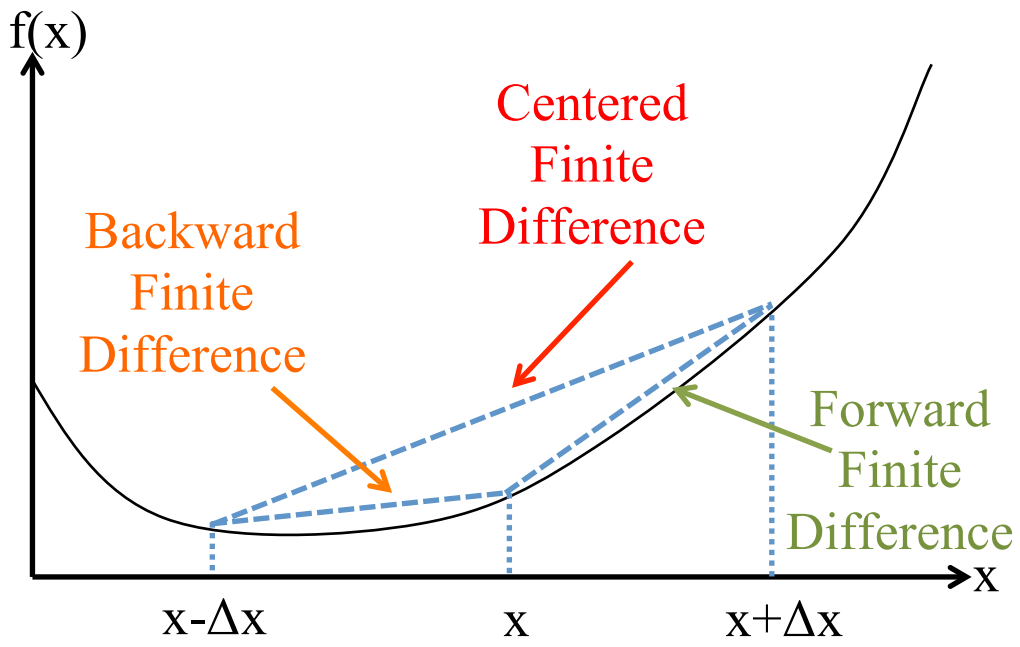

Figure 4.2. Geometrical representation of difference methods.

This is general approximation for first-order derivatives when the error is *O(*Δx*)*. Geometric representation of the forward (green arrow), backward (orange arrow) and centered (red arrow) finite difference forms are shown in Fig. 4.2.

Backward finite difference formula in discretized form for the node point can be calculated as;

$$\left(\frac{\partial f}{\partial x}\right)_i = \frac{f_i - f_{i-1}}{x-(x-\Delta x)} + O(x) = \frac{f_i - f_{i-1}}{\Delta x} + O(x) \qquad (4.12)$$

Using the equation (4.12), the advection term, giving the differential change in fluid velocity with respect to the change in axial distance, is represented as follows;

$$\frac{\partial T_f(z,t)}{\partial z} = \frac{T_f(z,t) - T_f(z-\Delta z,t)}{\Delta z} \qquad (4.13)$$

and thus temperature of fluid phase was determined at certain position with respect to time is shown using equation below;

$$T_f(z,t+\Delta t) = T_f(z,t) + \left[\underbrace{\left(\frac{-h(z,t).a.\left(T_f(z,t) - T(z,t)\right)}{\rho_f C_{p_f} \varepsilon} \right)}_{Fluid\,Convection} + \underbrace{\left(-v(z,t) \frac{T_f(z,t) - T_f(z-\Delta z,t)}{\Delta z} \right)}_{Fluid\,Advection} \right] \Delta t \qquad (4.14)$$

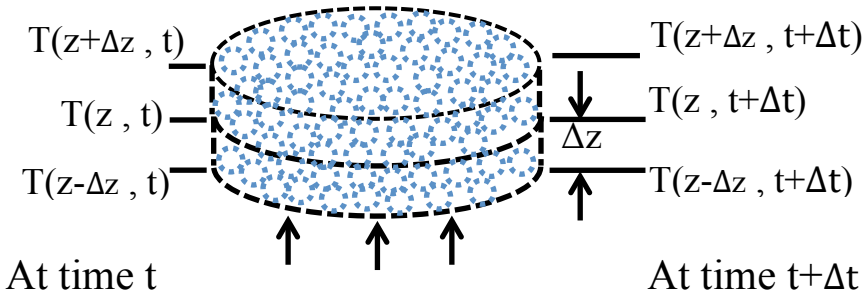

Figure 4.3. Schematic representation of the discretized variables to be used to write the partial differential equations in finite difference forms.

The discretization of the partial differential equations is illustrated schematically in Figure 4.3. The second order derivative, with respect to axial position, in the model equation representing the differential energy balance for the solid phase is discretized using the centered finite difference form.

$$\frac{\partial^2 f}{\partial x^2} = \frac{f(x+2\Delta x) - 2f(x+\Delta x) + f(x)}{(\Delta x)} + O(\Delta x) \tag{4.15}$$

Temperature change with respect to axial position was determined by the equations as follow;

$$\frac{\partial^2 T}{\partial z^2} = \frac{T(z+\Delta z, t) - 2T(z,\ t)\ + T(z-\Delta z,\ t)}{\Delta z^2} \qquad \text{at time t} \tag{4.16}$$

In addition, at the top of the TCES unit (z=L), there is no value of $T_S\,(L+\Delta z,\ t)$ term and this term becomes equal to $T_S\,(L,\ t)$. At this situation, the equation becomes;

$$\frac{\partial^2 T}{\partial z^2} = \frac{\left[-T(z,\ t)\ + T(z-\Delta z,\ t)\right]}{\Delta z^2} \quad at\ z = L, \quad T(L+\Delta z,\ \mathrm{t}) = T(L,\ \mathrm{t}) \tag{4.17}$$

Temperature of the solid at any position z, and time t+Δt was calculated by below given formula;

$$T(z,t+\Delta t) = T(z,t) + \frac{\partial T(z,t)}{\partial t}\Delta t \tag{4.18}$$

where temperature change for time wise is;

$$\frac{\partial T}{\partial t} = \underbrace{\left(k.\frac{T(z+\Delta z,t) - 2T(z,t) + T(z-\Delta z,t)}{\Delta z^2}\right)}_{Solid\ Conduction} + \underbrace{\left(\frac{-h_{conv}.a.\left(T_f(z,t) - T(z,t)\right)}{\rho_f C_{p_f}\varepsilon}\right)}_{Fluid\ Convection} + \underbrace{\frac{\partial C_{CaO}(z,t)}{\partial t}\frac{\Delta H_r}{\rho_S C_{p_S}}}_{Reaction} \tag{4.19}$$

Similar to the lumped parameter model, calcium oxide concentration was determined using the rate equation of Shao et al. (2013).

$$C_{CaO}(z,t+\Delta t) = C_{CaO}(z,t) + \frac{\partial C_{CaO}(z,t)}{\partial t}\Delta t \tag{4.20}$$

Water vapor flow rate for any location and time was determined using equation (4.21).

$$\dot{m}_{H_2O}(z,t) = \dot{m}_{H_2O}(z-\Delta z,t) - \Delta\dot{m}_{H_2O}(z-\Delta z,t) \tag{4.21}$$

where consumption rate of water vapor is;

$$\Delta\dot{m}_{H_2O}(z,t) = -\frac{\partial C_{CaO}(z,t)}{\partial t}.A_C.\frac{(1-\varepsilon)}{\varepsilon}Mw_{H_2O}\Delta z\,\Delta t \tag{4.22}$$

The axial position and time dependent state variables are the fluid and solid temperatures, CaO concentration and water vapor flow rate. The working fluid velocity, convective heat transfer coefficient and reaction rate constant are calculated for each position and time step using the computed values of the state variables. In the following section, the initial values and boundary conditions for the state variables will be explained briefly.

4.3 Initial Values and Boundary Conditions

The LPM equations are first order ordinary differential equations with respect to time. Therefore, only initial values of the state variables need to be known in order to start the computations. The DPM equations contain first order derivatives with respect to time, first and second order derivatives with respect to axial position. Thus, if the model equation contains only first order derivative with respect to axial position such as the advection term, a single boundary condition is necessary. However, when the model equation contains second order derivative with respect to axial position such as the thermal conduction term in the differential energy balance for the solid, two boundary conditions are required. The required initial values are given below.

$$t = 0,\ T(z,t) = T(z,0) = 373.15K$$
$$T_f(z,t) = T_f(z,0) = 373.15K$$
$$C_{CaO}(x,t) = C_{CaO}(x,0)$$

Initial temperatures both for the fluid and solid phases are set to be 100°C. The initial concentration of calcium oxide is calculated using the bulk density.

$$C_{CaO} = (1-\varepsilon).\frac{\rho_{CaO}}{MW_{CaO}} \quad t = 0 \tag{4.23}$$

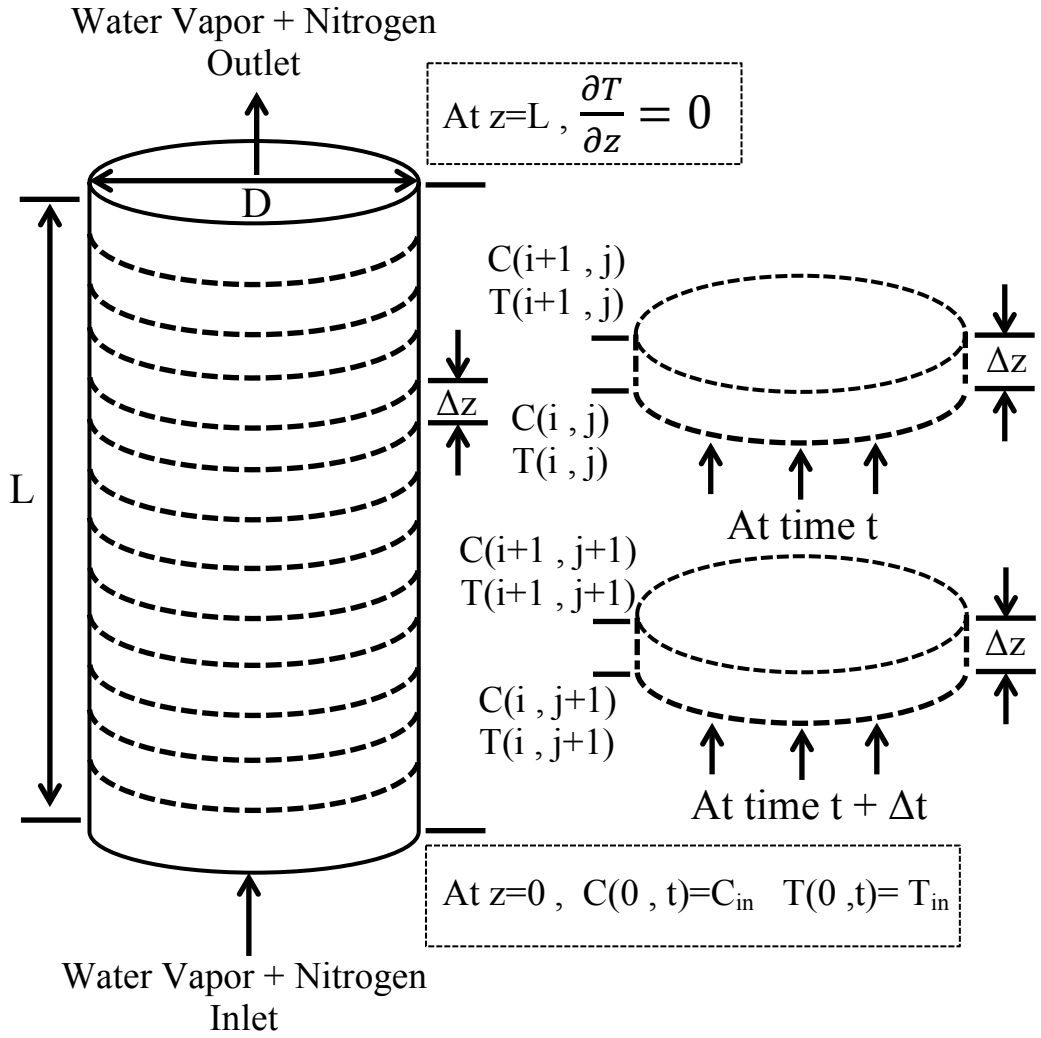

Figure 4.4. The schematic representation of model in present work.

The discretization and the boundary conditions for the DPM are shown in Fig. 4.4. The fluid temperature at the inlet of the TCES unit is fixed (boundary condition) and the solid temperature at the inlet is calculated using the differential energy balance equation for the solid phase. It means that the water reservoir was kept at constant

temperature of the working fluid.

$$z = 0 \qquad T_f(0,t) = T_{in}$$

At the exit of the TCES unit, no boundary condition is required for the fluid phase. However, the symmetry or no transfer boundary condition is needed for the solid phase at the exit of the TCES unit.

$$z = L \qquad \left.\frac{\partial T}{\partial z}\right|_{z=L} = 0$$

TCES unit (z=L) there is no heat transfer.

CHAPTER 5

RESULTS AND DISCUSSION

Distributed and lumped parameter models were solved for better understanding of thermochemical energy storage using hydration reaction of CaO and results plotted for different parameters and model separately. In this chapter results will be explained in detail and parameter will be discussed for each situation concerning graphs.

5.1. Results of the Lumped Parameter Semi Batch Model

On Fig. 5.1, the hydration reaction rate of CaO using the kinetics data of Fujimoto et al. (2002) was plotted. According to Fig. 5.1, reaction rate using the rate expression of Fujimoto et al. (2002) increases continuously even if temperature of the reaction media reaches above 753K which is equilibrium temperature under the pressure of 1 atm.

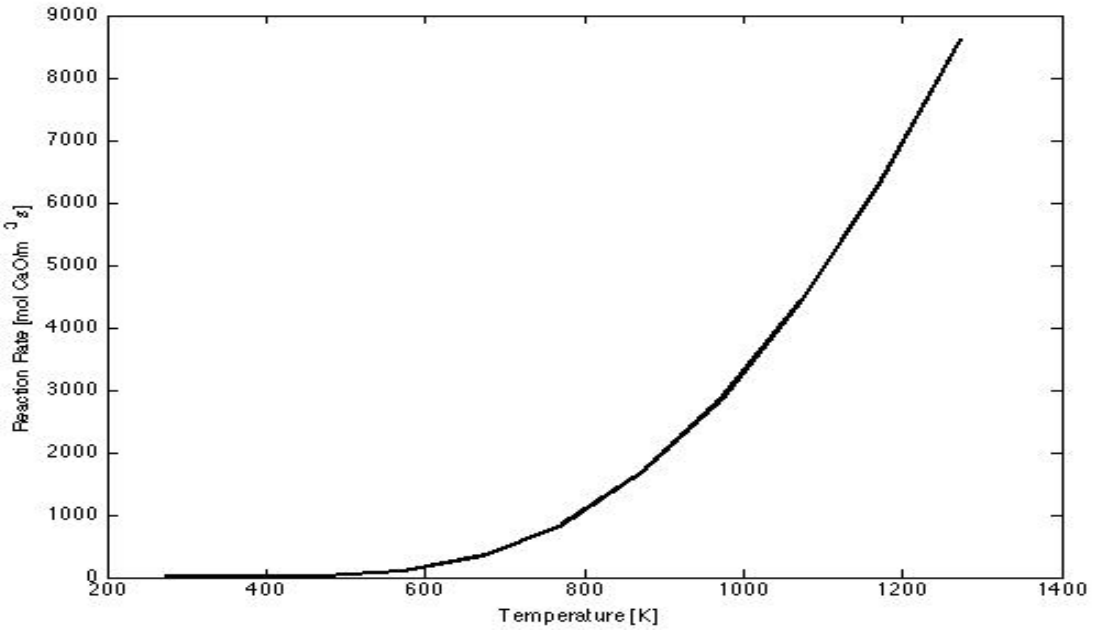

Figure 5.1. Reaction rate as a function of temperature using the rate expression of Fujimoto et al. (2002).

The reaction rate rapidly increases according to the rate equation of Shao et al. (2013) in Fig. 5.2. The difference between these two figures are due to the equilibrium temperature which was not considered in the rate equation of Fujimoto et al. (2002). That is why reaction rate increases as temperature increases according to Fujimoto et al. (2002) without any effect of the equilibrium temperature. In reality, the dehydration reaction progresses above the equilibrium temperature.

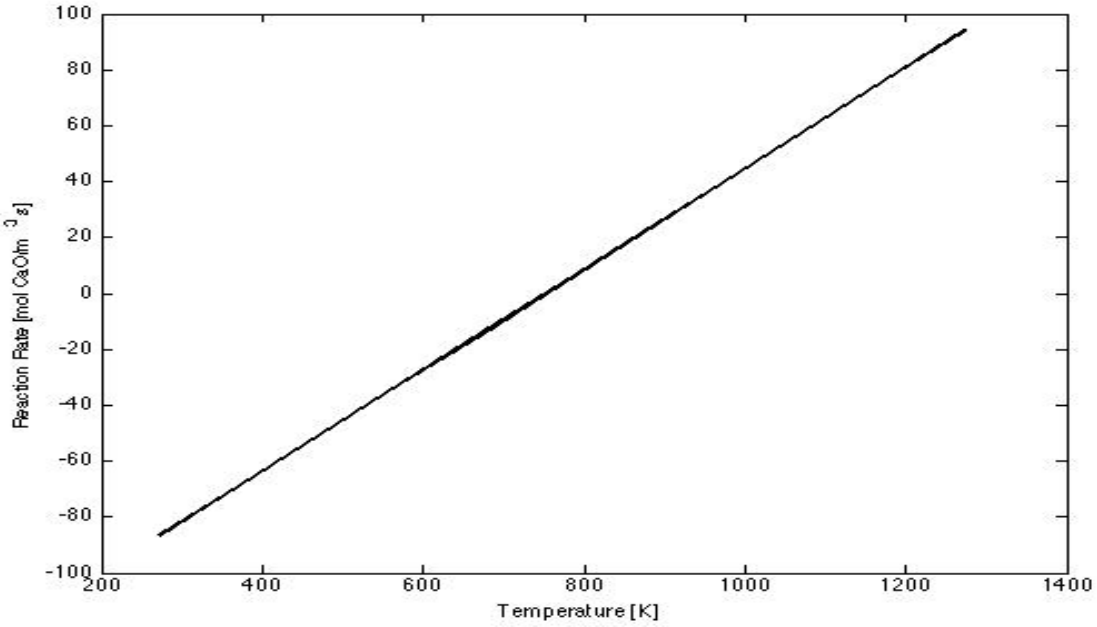

Figure 5.2. Reaction rate as a function of temperature using the rate expression of Shao et al. (2013).

On the contrary, according to the rate equation proposed by Shao et al. (2013), the reaction rate slows down as shown on Fig. 5.2, and becomes equal to zero when the equilibrium temperature at about 753.23 K was reached. The reaction rate becomes positive above 753.23 K which means increasing temperature favors the dehydration reaction. Simulations for a semi batch TCES unit were realized using the reaction rate expression proposed by Shao et al. (2013) and the results were presented by figures 5.3-5.6 In Fig. 5.3, the CaO concentration profile was plotted as a function of time. The CaO concentration decreases from 18 to 11 kmol/m^3 after about 30 minutes. Because temperature of reaction media reaches the equilibrium temperature of 753.23 K as shown in Fig. 5.4.

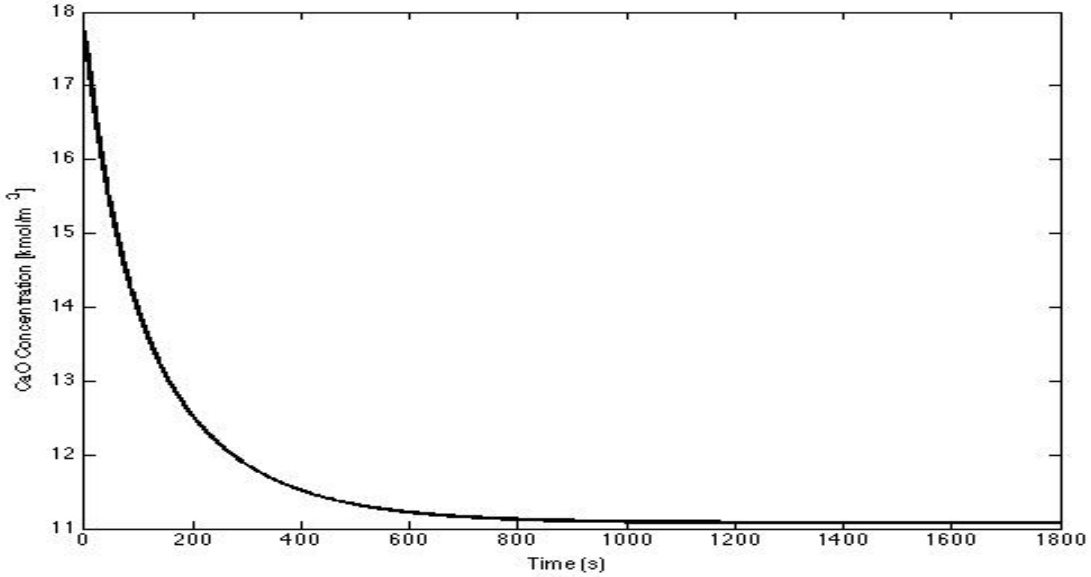

Figure 5.3. CaO concentration profile as a function of time according to the rate equation proposed by Shao et al. (2013)

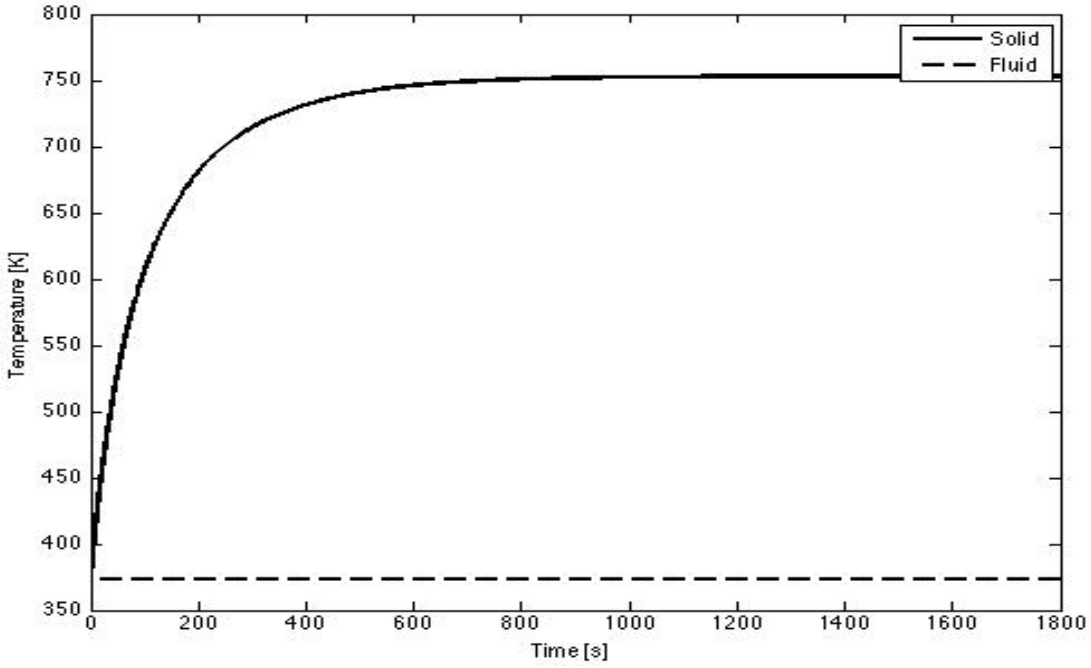

Figure 5.4. Temperature profile as a function of time according to the rate equation proposed by Shao et al.

In the semi batch lumped parameter model, there is no heat removal from the TCES unit. That is why the temperature continues rising as the reaction progresses until the equilibrium temperature. This figure shows us the importance of heat removal from the TCES during the exothermic hydration reaction. The water vapor flow rate required as shown in Fig. 5.5, was calculated based on the rate of the hydration reaction. This is another important curve showing the importance of the water vapor supply rate. Controlling the water vapor supply rate can control the progress of the hydration reaction. Thus one can easily adjust the reaction rate and the temperature by manipulating the water vapor flow rate.

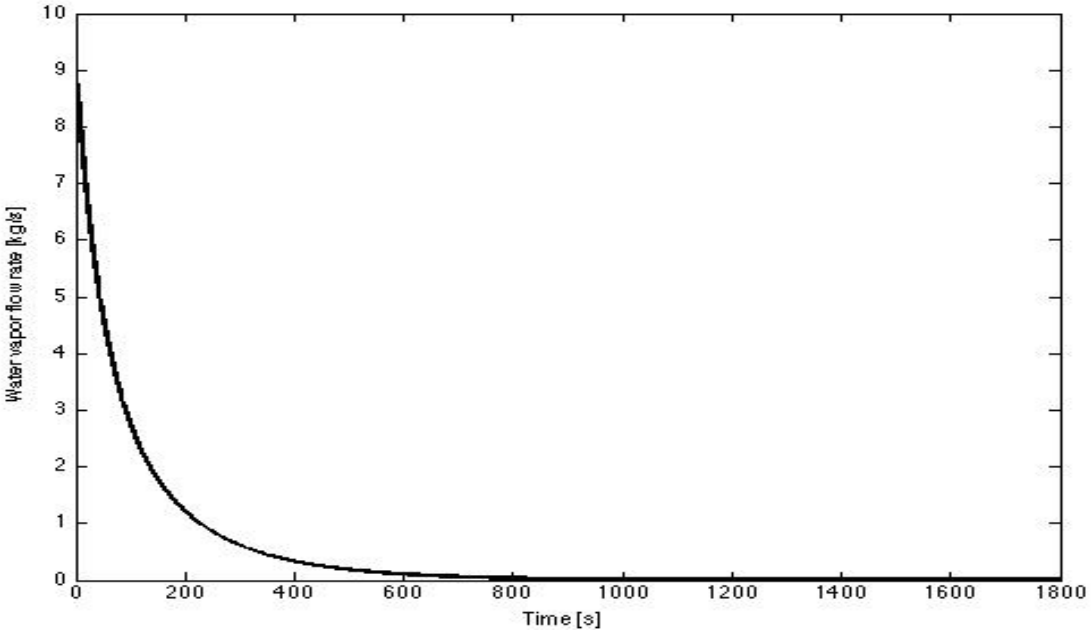

Figure 5.5. Required water vapor flow rate as a function of time according to the rate equation proposed by Shao et. al.

Similar to the figures 5.4 and 5.5, Fig. 5.6 shows the maximum limit of the heat removal rate during the hydration reaction. In the design of the TCES this is another design parameter to be taken into account to obtain a certain amount of heat at a certain temperature.

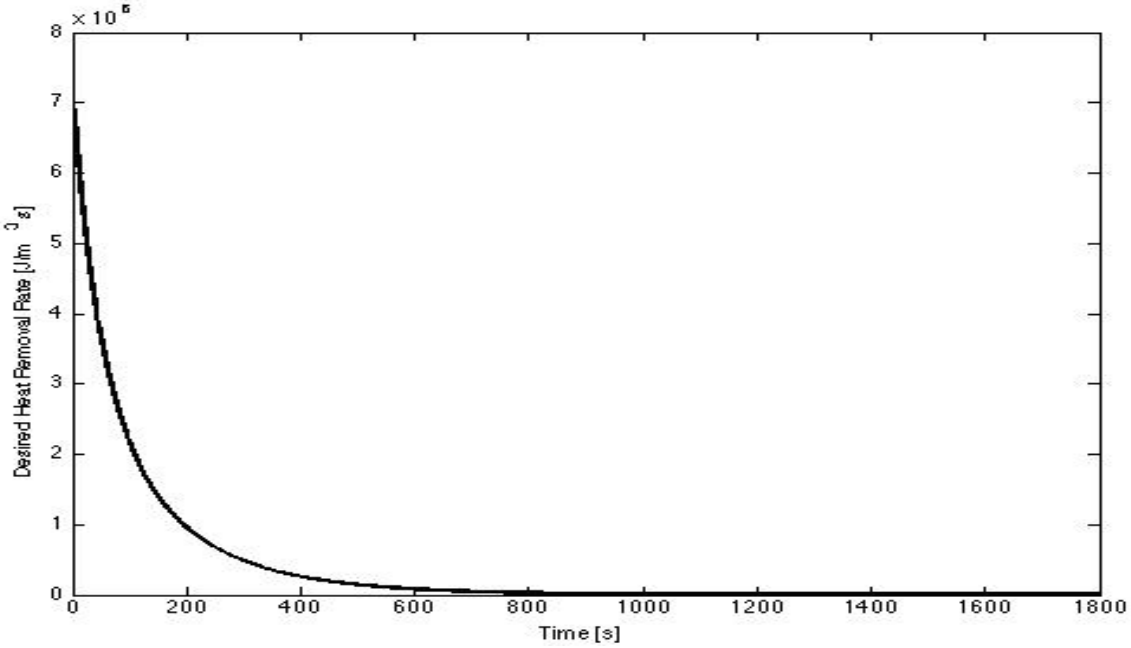

Figure 5.6. Desired heat removal rate as a function of time according to the rate equation proposed by Shao et. al.

5.2. Results of the Distributed Parameter Semi Batch Model

The results of the distributed parameter model are discussed in detail in the following paragraphs.

Table 5.1 The parameters used in the simulations to give the figures 5.7 – 5.17.

Parameter	Symbol	Units	Value
Height	L	m	1.0
Diameter	D	m	0.5
Void fraction	ε	-	0.5
Particle diameter	d_p	m	0.003
Working fluid inlet temperature	$T_{if\ in}$	K	373.15
Water vapor inlet flow rate	$m_{wv\ in}$	kg/s	0.0174
Nitrogen inlet flow rate	$m_{N2\ in}$	kg/s	0.0035

Important dimensionless numbers such as Reynolds, Nusselt and Biot numbers were investigated as well as operation variables. Moreover, macroscopic energy balance was computed for better understanding of heat recovery. For different conditions and dimension of TCES unit, results are performed and shown in this chapter. Parameters used for results in relevant part of this chapter, are shown in Table 5.1.

Solid and fluid temperatures during the simulations were given by figures 5.7 and 5.8, respectively. The temperature profiles for the fluid and solid phases show the same trend of heat front propagation similar to the formation of waves in a sea.

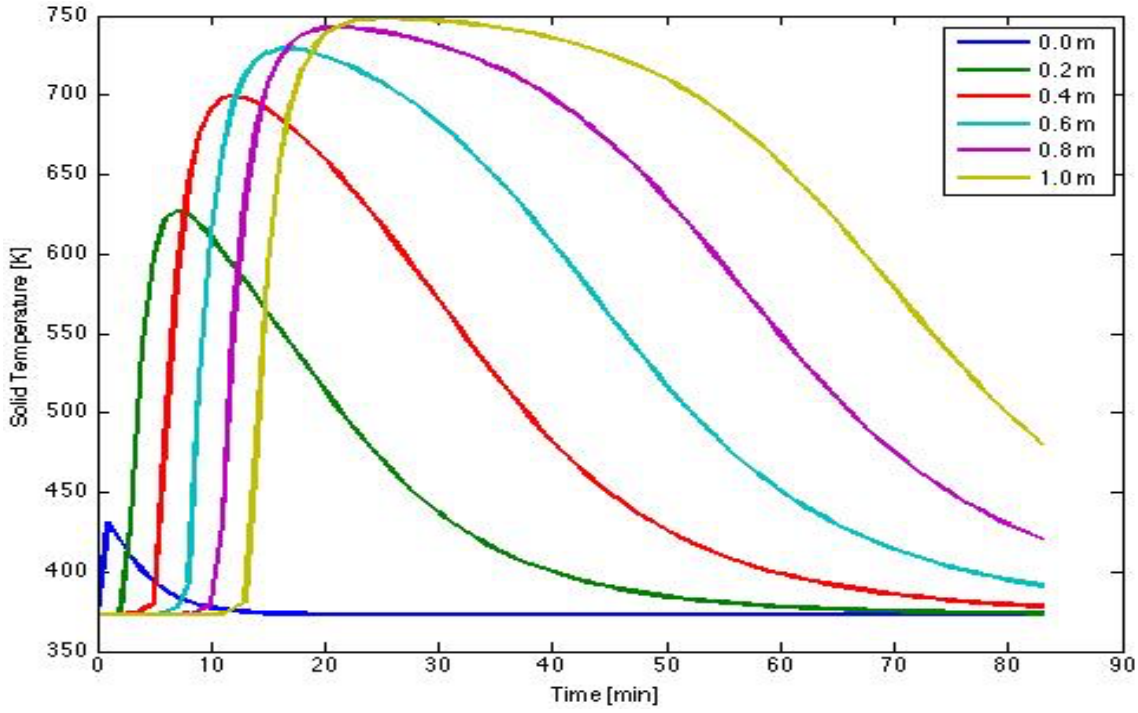

Figure 5.7. Solid temperature profiles at different height.

Distributed parameter model was developed according to the desired height of TCES unit and time. Strong evidence of Fig 5.7 indicates that temperature of solid increases until around 750 K due to the heat carried by the working fluid between the bottom and top of the heat storage unit. Those waves show a variation at different points. In figure 5.7 and 5.8, the blue and the yellow lines refer to the entrance (bottom) point and exit (top) of the TCES unit, respectively. As it can be seen on Fig 5.8, initially

working fluid temperature is constant along the bed. On the other hand, the fluid temperature increases through the length of bed as the reaction proceeds. First point (at 0.2 m) increases faster and cools down rapidly compared to the upper levels in the TCES unit. Furthermore, the higher levels, close to the top reach to higher temperatures, cool down gradually and slower compared to the lower levels.

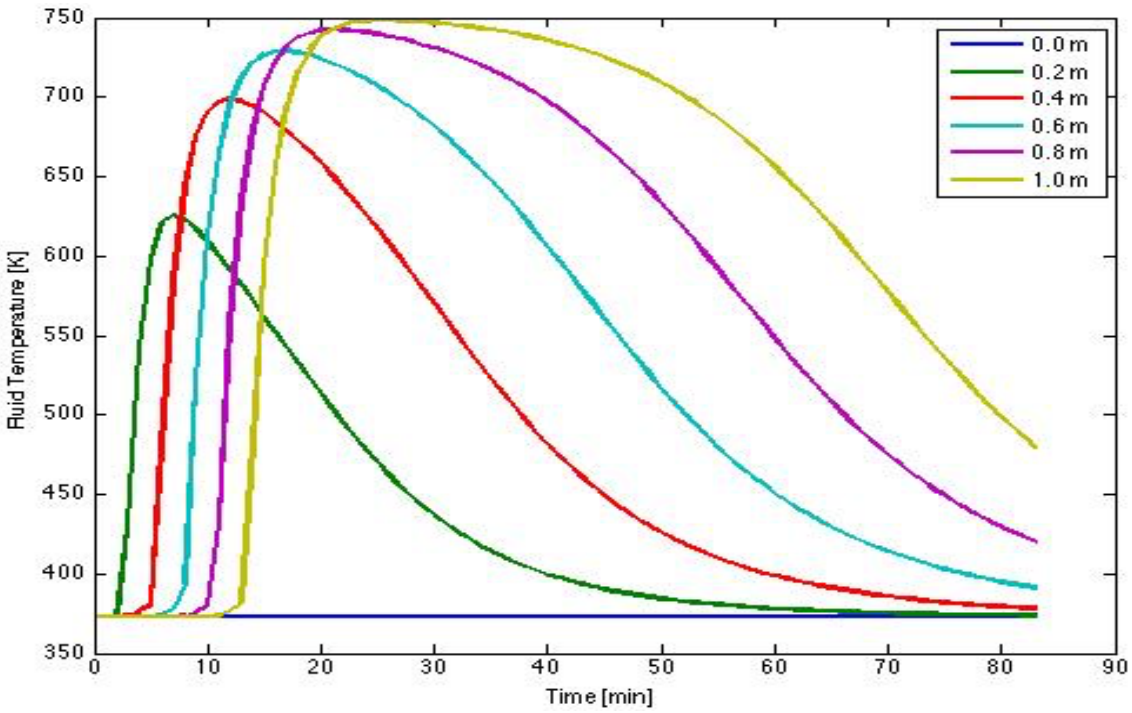

Figure 5.8. Fluid temperature profiles at different height.

The results, as seen in Fig 5.8, represent that fluid temperature, similarly to solid temperature, increases and decreases with respect to time. That effect is caused by the contact of water vapor with CaO and reaction heat released by the hydration of CaO. The solid and fluid temperatures reach almost to the thermodynamic equilibrium temperature between 25 and 50 minutes at the top of the bed.

Figures 5.9 and 5.10 together illustrate the increase in the reaction rate and the effect of the vapor available. Through the reaction chamber, vapor mass flow rates at different heights are shown in Fig 5.9. The water vapor is consumed almost instantaneously (as soon as it enters the TCES at the bottom) at the beginning of the hydration. That is why the water vapor flow rate is zero at the exit of the TCES unit for the first 12 minutes of the operation. Figures 5.9 and 5.10, together show the

change of vapor flow rates and also show that there is a reaction front moving towards the top of the bed. The reaction rate is controlled by the vapor mass flow rate available. The blue line represents the inlet water vapor mass flow rate.

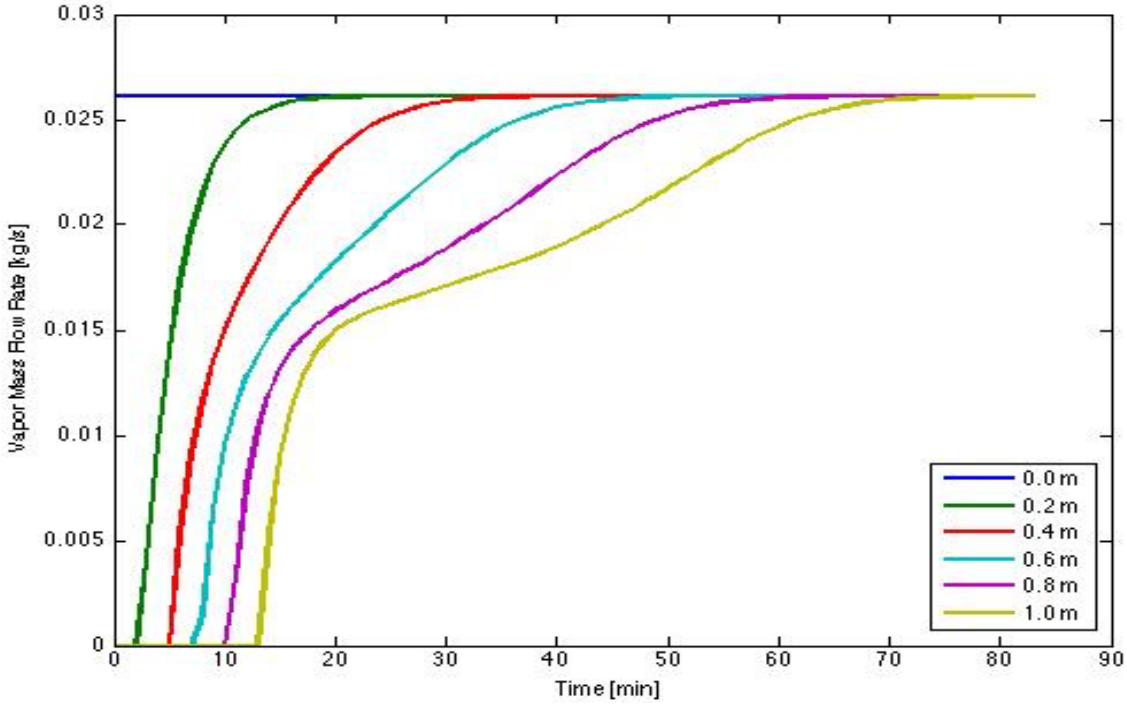

Figure 5.9. Vapor mass flow rate as a function of time at different height.

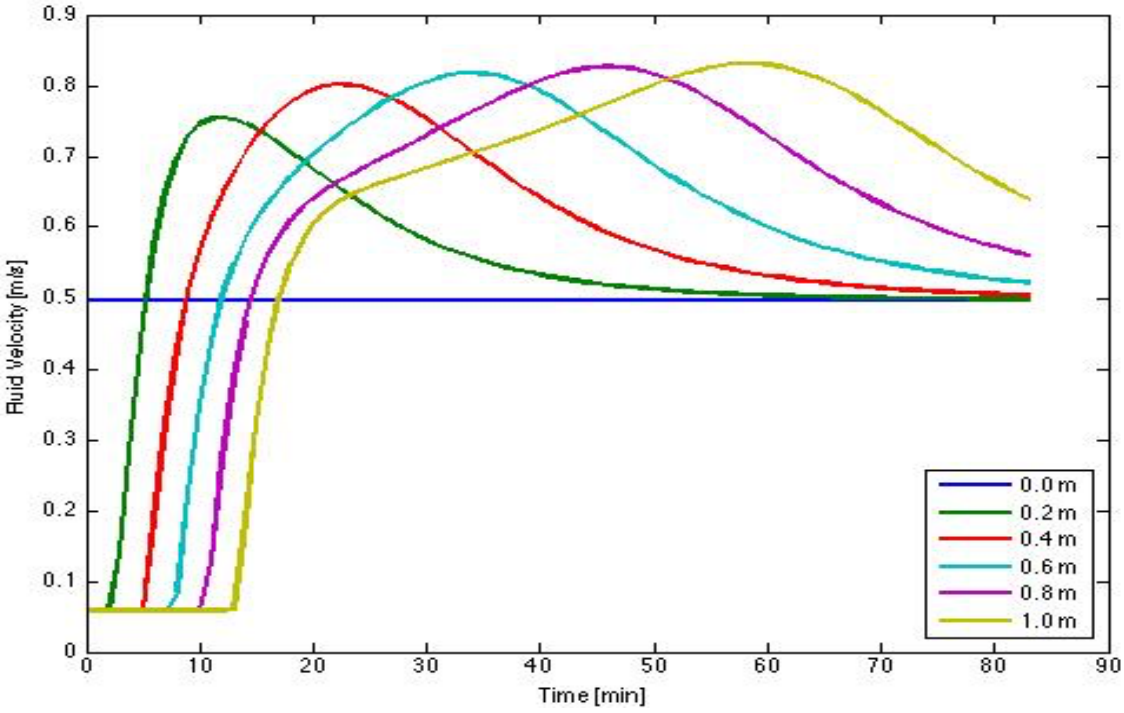

Figure 5.10. Fluid velocity rate as a function of at different height.

In this study, as working and heat transfer fluid, a mixture of water vapor and nitrogen is supplied to the TCES unit. Until around 13-14 minutes, there is no water vapor available at the top of the bed, Fig. 5.9. As time passes, temperature increases and decreases and thus the working fluid velocity as shown in Fig. 5.10, follows the similar waves to the temperature profiles and eventually reaching the velocity at the inlet conditions. So it is clear that the reaction front propagation similar to the domino effect and it is easily visible in all figures representing the dynamic variation of the state variables used in the model.

Variation of the CaO profiles along time due to water vapor availability and temperature reached around the thermodynamic equilibrium temperature during hydration is shown in Fig. 11. When Fig. 11 is considered, the blue line is the entrance point, is used up first because of contact time with the water vapor.

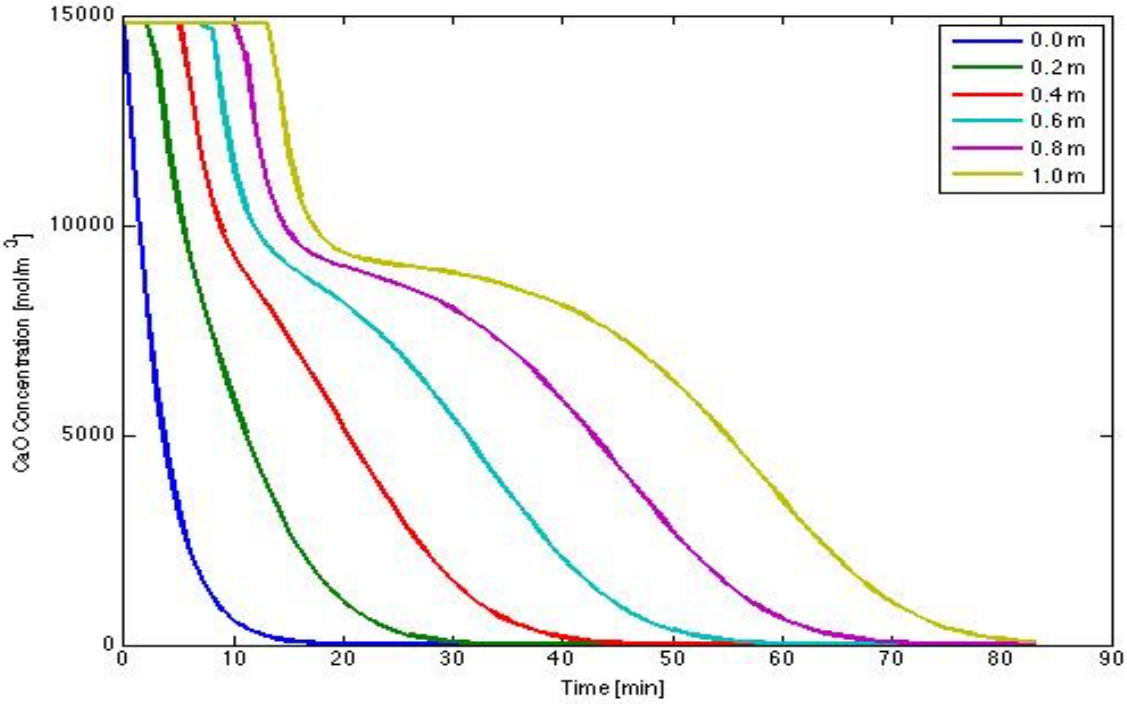

Figure 5.11. CaO concentration profile for different height.

The reaction rate is the time derivative of CaO profiles and thus reaction rate along the packed bed shows variations caused by variations of CaO concentration and temperature. This situation causes reaction rate waves along the reactor. At the upper levels of the heat storage unit, the reaction rate increases and decreases as the

equilibrium temperature is reached. These results provide confirmatory evidence that equilibrium temperature prohibits the rate of hydration reaction. As the heat is removed from the system the reaction rate increases again.

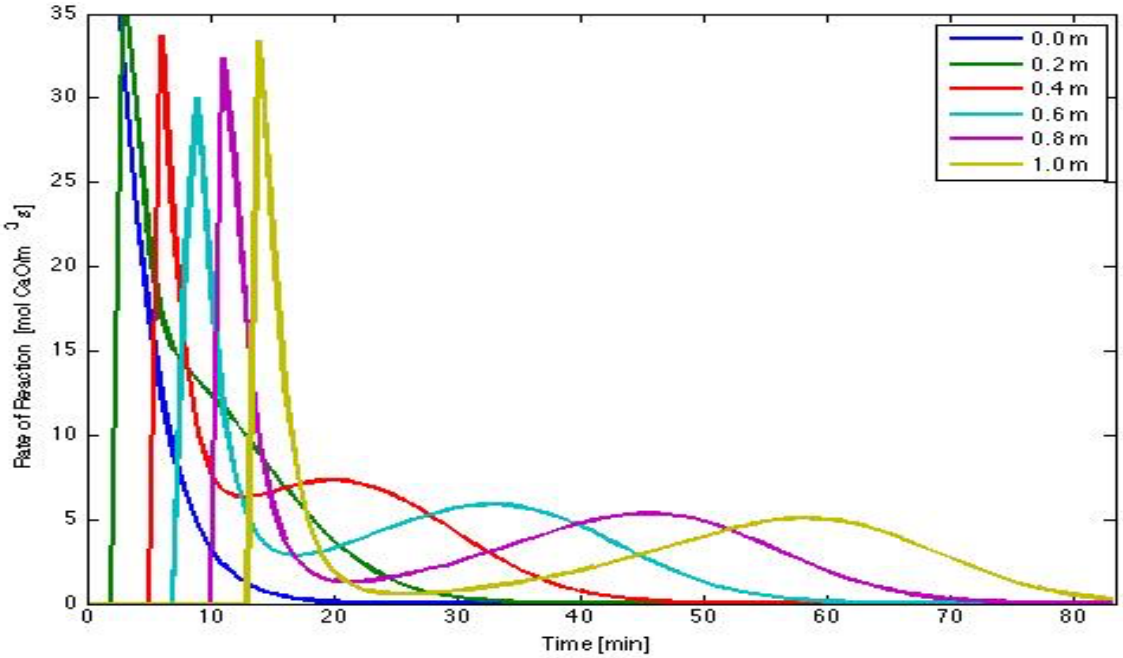

Figure 5.12. Reaction rate profile for different heights. .

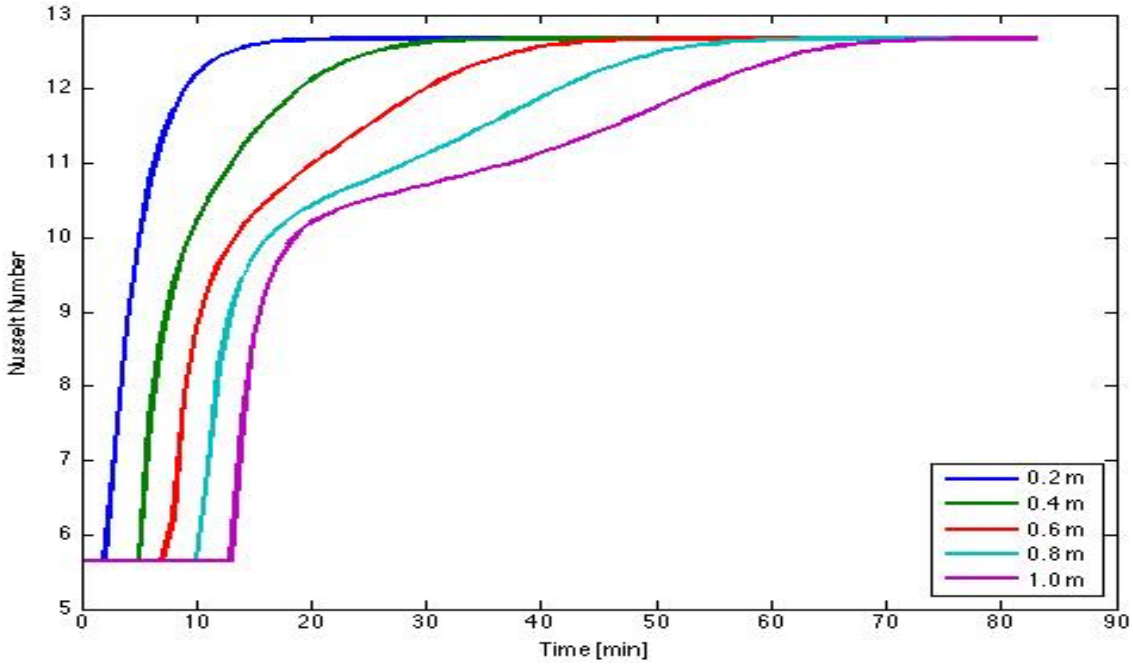

Figure 5.13. Nusselt number profile.

Nusselt and Reynolds numbers profiles are shown in figures (5.13) and (5.14), respectively. As the reaction progresses less water vapor is consumed. Thus, the working fluid flow rate increases with time and this causes the velocity of the fluid to increase, figures (5.9) and (5.10). Due to the increase in the fluid velocity, Reynolds number increases as shown on Fig. 5.14 and reaches a constant value of around 10 as the hydration of CaO is completed. Higher Reynolds numbers correspond to higher Nusselt numbers and thus higher convective heat transfer coefficients.

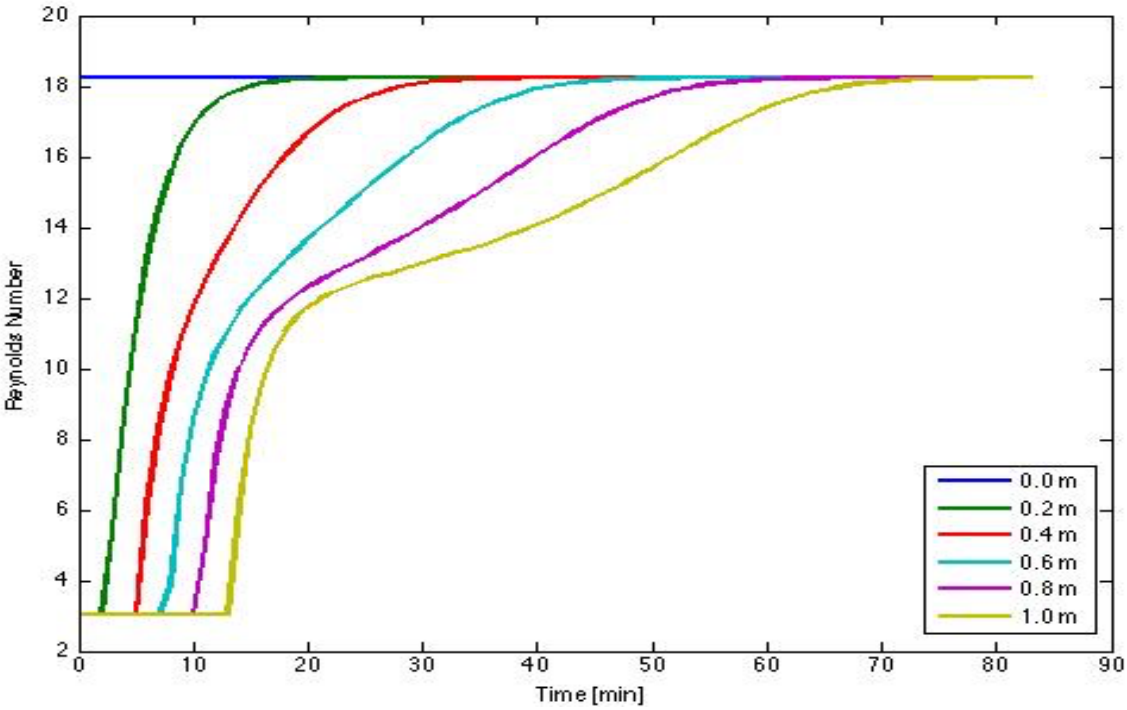

Figure 5.14. Reynolds number profile.

Convective heat transfer coefficient as a function of time is shown in Fig. 5.15. Concerning Fig. 5.15, convective heat transfer coefficient varies between 150 and 350 during 80 minutes. It increases and remains constant at around 350 J/m^2 s K. Increasing of convective heat transfer coefficient is proportional to Nusselt and Reynolds numbers.

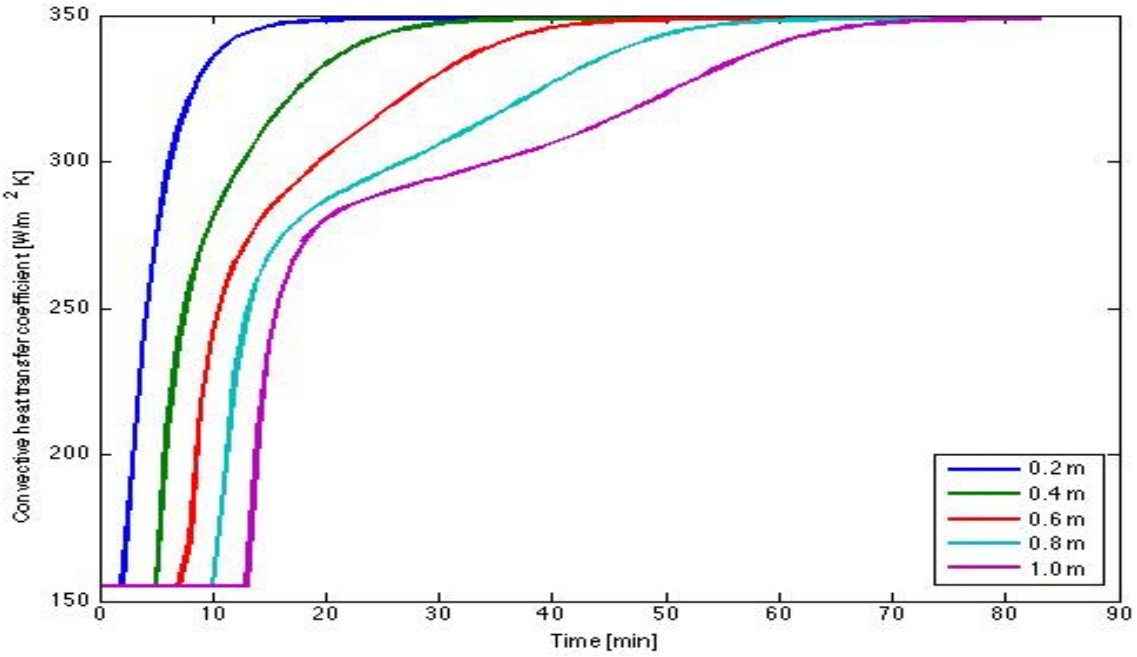

Figure 5.15. Convective heat transfer coefficient profile.

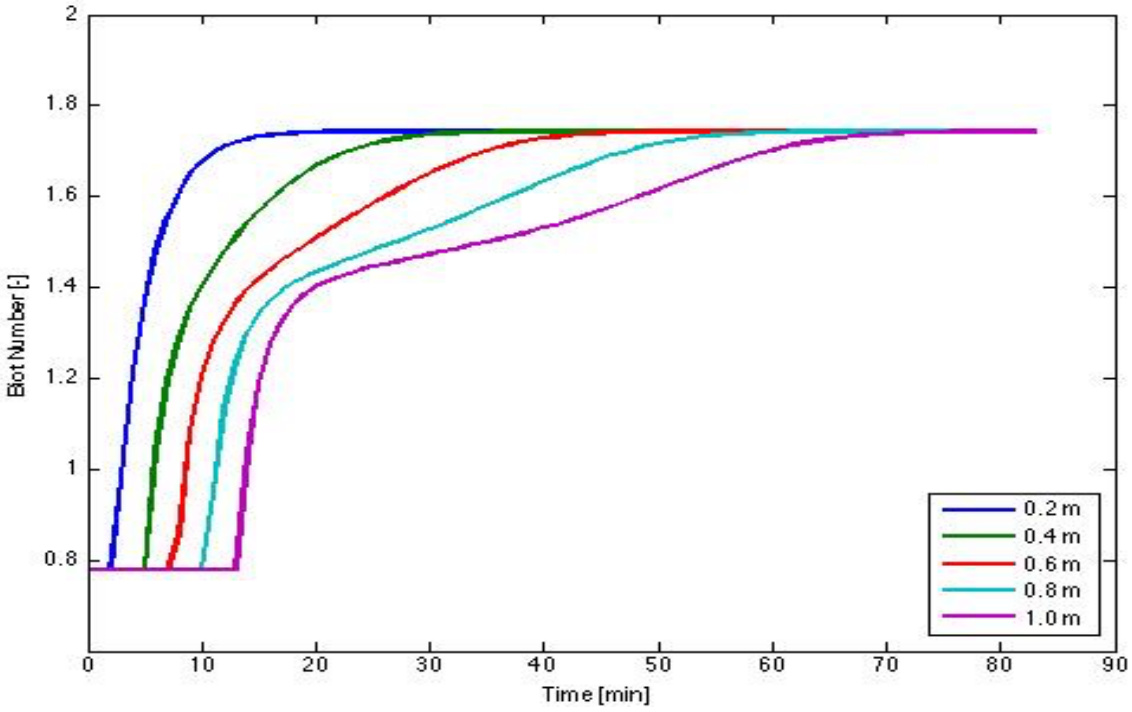

Figure 5.16. Biot number profiles.

The variation of the Biot number was shown on Figure 5.16. The particle diameter used in the computations was chosen to be 3 mm. The effect of temperature gradient within the particles starts to become slightly important as the Biot number is above

1.0. Fig. 5.16 shows that temperature distribution within the particles is not uniform. However the effect of the temperature gradients within the particle are not drastic as the maximum value of the Biot number computed is less than 1.8.

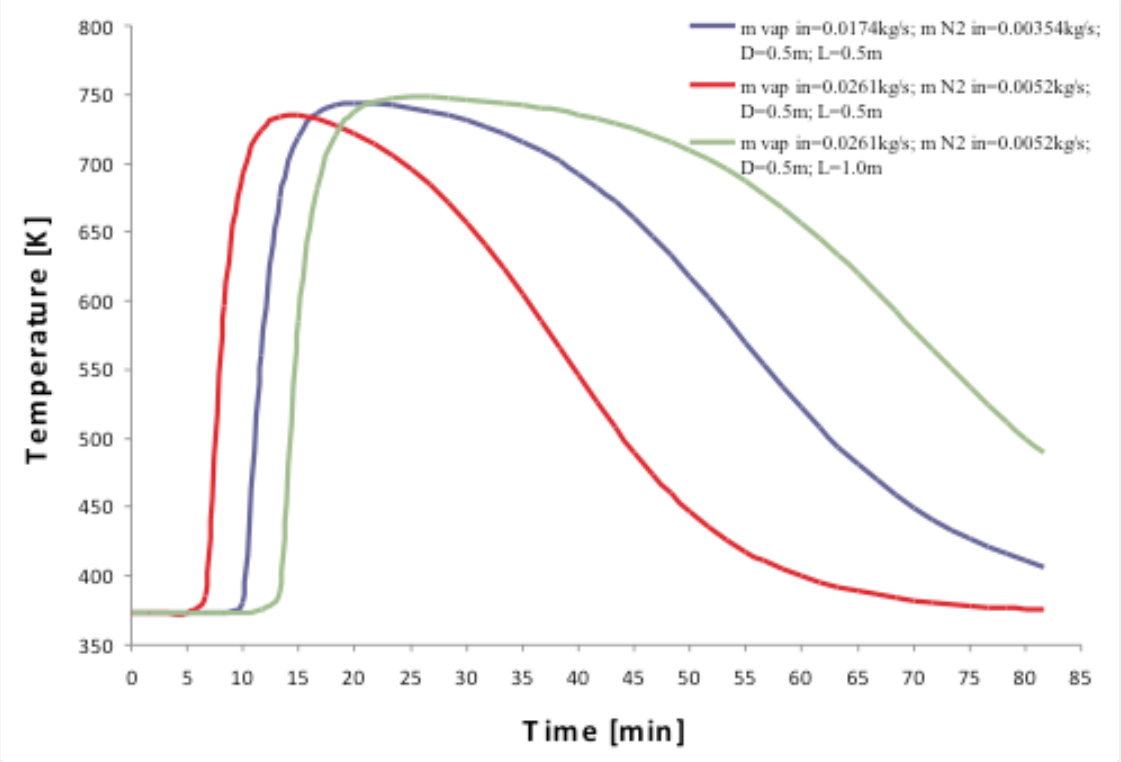

Figure 5.17. Outlet temperature profiles for different simulations varying the inlet vapor flow rate, inlet nitrogen flow rate, and bed height.

Different simulations were performed for different design and working parameters. Simulation results are shown in Fig. 5.17 for different water vapor and nitrogen inlet flow rate and also two different heights. Desired energy production rate requires optimization of design parameters such as diameter, height and particle diameter . In the same manner, water vapor inlet flow rate, nitrogen flow rate and inlet temperature are operating parameter of the system. These parameters determine maximum temperature to be reached and time of energy production period. As clearly seen in figure above, increasing working fluid flow rate increases reaction rate and outlet fluid temperature reaches around equilibrium temperature then decreases gradually. Increasing the height keeps fluid at high temperatures as wide as possible. Inlet conditions can be adjusted as a function of time for desired purpose.

6. CONCLUSION

The purpose of the present research is to develop mathematical model for thermochemical energy storage using hydration reaction of calcium oxide (CaO) and computed by Matlab ® software numerically. Lumped and distributed parameter model were used separately to simulate a TCES unit and to obtain the profiles of temperature, concentration and reaction rate for a semi batch open direct concept thermochemical energy storage.

Simulations of the LPM were done for two different rate equations. Rate equation of Fujimoto et al. (2002) was showed increase on temperature continuously. This situation was observed due to the equilibrium temperature was not considered in the rate equation of Fujimoto et al. (2002). The reaction rate rapidly increased according to the rate equation of Shao et al. (2013). When using the hydration rate equation proposed by Shao et. al., temperature reached around 750 K (thermodynamic equilibrium temperature) and kept constant at this temperature. Concerning progress of the hydration reaction can be controlled by controlling the water vapor supply rate, it is possible to hypothesize that one can easily adjust the reaction rate and the temperature by manipulating the water vapor flow rate. The CaO concentration varied between 18 and 11 kmol/m^3 after about 30 minutes due to temperature around 750 K. Temperature showed a continuous increase as the reaction progresses until the equilibrium temperature.

The DPM results show that the working fluid temperature increased until around 700 K during hydration. Solid phase temperature also increased and then decreased similar to the fluid temperature. In approximately 25 and 50 minutes the solid and fluid temperatures of top of the bed reach almost to the thermodynamic equilibrium. Until around 13-14 minutes, water vapor was almost used up. The reaction rate was fluctuated due to equilibrium temperature was reached. As the heat removed by the working fluid temperature decreased below the equilibrium temperature and thus reaction rate started to increase again.

Simulation results showed lumped parameter model can be used to simulate the process or small size chemical heat storage units for small size chemical heat storage units. Contrary, distributed parameter model should be used for larger chemical heat

storage units. Consequently design parameters and operating parameters should be set for different purposes.

Future research should be done to investigate the operation ranges of the optimization variables such as the flow rates of the water vapor and heat transfer fluid by improved model. There is no design about efficient use of a TCES unit currently. But by means of simulation results of developed models, pre designs are possible. In order to realize industrial applications, a TCES unit should be designed in a pilot scale.

REFERENCES

1. Abedin A. H. (2010) Thermochemical Energy Storage Systems: Modelling, Analysis and Design, M. Sc. Thesis, University of Ontario Institute of Technology, Oshawa, Ontario, Canada.

2. Abedin A. H., M. Rosen A. (2011), "A critical review of thermochemical energy storage systems", The Open Renewable Energy Journal 4, 42-46.

3. Abedin, A. H., and Rosen, M. A. (2012), "Closed and open thermochemical energy storage: Energy- and exergy-based comparisons", Energy, 41, 83-92.

4. Azpiazu M.N., Morquillas J.M., Vazquez A. (2003), "Heat recovery from a thermal energy storage based on the $Ca(OH)_2/CaO$ cycle", Applied Thermal Engineering, 23, 733–741.

5. Céspedes, E., Wirz, M., Sánchez-García, J. A., Alvarez-Fraga, L., Escobar-Galindoa, R., and C. Prieto (2014) Novel Mo–Si_3N_4 based selective coating for high temperature concentrating solar power applications", Solar Energy Materials & Solar Cells 122, 217–225.

6. Çengel, Y.A., Boles, M.A., (2012) Termodinamik (Mühendislik Yaklaşımıyla), Güven Bilimsel Yayıncılık, İzmir, Türkiye.

7. Department of Energy and Climate Change, U.K. Government (2013), https://www.gov.uk/government/uploads/system/uploads/attachment_data/file/65954/chapter_3_domestic_factsheet.pdf

8. Dinçer, İ., Rosen, M. A. (2011) Thermal Energy Storage Systems and Applications, Second Edition, A John Wiley and Sons, Chichester, United Kingdom.

9. Evcil, A.(2012) An estimation of the residential space heating energy requirement in Cyprus using the regional average specific heat loss coefficient, Energy and Buildings 55, 164–173.

10. Faninger, G. "Thermal Energy Storage", IFF – University of Klagefurt, Austria, http://celsius.co.kr/phase_change_materials/download/energy/Thermal_Energy_Storage.pdf (N/A)

11. Fujimoto S., Bilgen E., Ogura H. (2002) Dynamic simulation of CaO/Ca(OH)2 chemical heat pump systems'', Exergy, an International Journal 2, 6–14.

12. Hänchen M., Brückner S., Steinfeld A. (2011) High-temperature thermal storage using a packed bed of rocks e Heat transfer analysis and experimental validation, Applied Thermal Engineering 31, 1798-1806.

13. J. Xu, R.Z. Wang, Y. Li, (2013) A review of available technologies for seasonal thermal energy storage, Solar Energy ,103, 610-638

14. K. Edem N'Tsoukpoe, Hui Liu, Nolwenn Le Pierre`s, Lingai Luo (2009) A review on long-term sorption solar energy storage, Renewable and Sustainable Energy Reviews 13, 2385–2396.

15. Kazanasmaz, T., Erlalelitepe Uygun, I., Akkurt, G. G., Turhan, C., and Ekmen, K. E. (2014) On the relation between architectural considerations and heating energy performance of Turkish residential buildings in Izmir, Energy and Buildings, 72, 38–50.

16. Lee, T., "Latent and sensible heat storage in concrete blocks", M. Sc. Thesis, Concordia University, Montreal, Quebec, Canada, October 1998, http://spectrum.library.concordia.ca/728/1/MQ39095.pdf

17. Mawire A., McPherson M., R.R.J. Heetkamp van den, Mlatho S.J.P. (2009) Simulated performance of storage materials for pebble bed thermal energy storage (TES) systems, Applied Energy 86, 1246–1252.

18. Mehling, M., Cabeza, L.F., (2008) Heat and Cold Storage with PCM: An up to Date Introduction Into Basics and Applications, 1st Edition., Springer, Berlin Heidelberg, Germany.

19. N'Tsoukpoe K. E., Liu H., Le Pierre`s N., Luo L. (2009) A review on long-term sorption solar energy storage'', Renewable and Sustainable Energy Reviews 13 2385–2396.

20. Ogura H., Ishida H., Yokooji R., Kage H., Matsuno Y., Mujumdar A. S. (2001) Experimental studies on a novel chemical heat pump dryer using a gas–solid reaction, Drying Technology: An International Journal, 19(7), 1461–1477.

21. Ogura H., Mujumdar A. S. (2000) Proposal For A Novel Chemical Heat Pump Dryer, Drying Technology: An International Journal, 18(4&5), 1033-1053.

22. Ogura H., Yamamoto T., Kage H., Matsunoa Y., A. Mujumdar S. (2002) Effects of heat exchange condition on hot air production by a chemical heat pump dryer using $CaO/H_2O/Ca(OH)_2$ reaction, Chemical Engineering Journal, An International Journal 86, 3–10.

23. Ogura, H., Shimojyo R., Kage H., Matsuno Y. & Mujumdar A. S. (1999) Simulation of hydration/dehydration of CaO/Ca(OH)2 chemical heat pump reactor for cold/hot heat generation Drying Technology: An International Journal, 17(7&8), 1579-1592.

24. P. Pardo, A. Deydier, Z. Anxionnaz-Minvielle, S. Rougé, M. Cabassud, P. Cognet, (2014) A review on high temperature thermochemical heat energy storage, Renewable and Sustainable Energy Reviews. 32, 591–610.

25. Portaspana J. C. (2011) High temperature thermal energy storage systems based on latent and thermo-chemical heat storage, M. Sc. Thesis, Technischen Universität Wien Faculty of Mechanical and Industrial Engineering, Karlsplatz, Vienna, Austria.

26. Schaube F., Koch L., Wörner A., Müller-Steinhagen H. (2012) A thermodynamic and kinetic study of the de- and rehydration of Ca(OH)2 at high H2O partial pressures for thermo-chemical heat storage, Thermochimica Acta 538, 9–20.

27. Schaube F., Koch L., Wörner A., Müller-Steinhagen H. (2012) Thermodynamic and kinetic study of the de- and rehydration of Ca(OH)2 at high H_2O partial pressures for thermo-chemical heat storage'', Thermochimica Acta 538, 9–20.

28. Schaube F., Kohzer A., Schütz J., Wörner A., Müller-Steinhagen H. (2013) De- and rehydration of $Ca(OH)_2$ in a reactor with direct heat transfer for thermo-chemical heat storage. Part A: Experimental results, Chemical Engineering Research and Design 91, 856–864.

29. Schaube F., Utz I., Wörner A., Müller-Steinhagen H. (2013) De- and rehydration of Ca(OH)2 in a reactor with direct heat transfer for thermo-chemical heat storage. Part B: Validation of model, Chemical Engineering Research and Design 91,

865–873.

30. Schmidt M., Szczukowski C., Roßkopf C., Linder M., Wörner A. (2014) Experimental results of a 10 kW high temperature thermochemical storage reactor based on calcium hydroxide, Applied Thermal Engineering, 62, 553-559.

31. Setterwall, F., Alexanderson, K. (1996) Phase change materials and chemical reactions for thermal energy storage, Royal Institue of Technology, Sweden.

32. Shao H., Nagel T., Roßkopf C., Linder M., Wörner A., Kolditz O. (2013) Non-equilibrium thermo-chemical heat storage in porous media: Part 2 e A 1D computational model for a calcium hydroxide reaction system, Energy 60, 271-282.

33. Zamengo M., Ryu J., Kato Y. (2014) Thermochemical performance of magnesium hydroxide-expanded graphite pellets for chemical heat pump, Applied Thermal Engineering 64, 339-347.

ÖZGEÇMİŞ

Kişisel Bilgiler

Adı Soyadı:	**Ender ERCAN**
Doğum Yeri ve Tarihi:	**İstanbul / 15.10.1988**
Adress:	**Ortaçeşme Tuna Sokak No: 40 / 4**
	Beykoz / İSTANBUL
Email:	**endererc@gmail.com**

Öğrenim Durumu

2002 – 2006	**Fevzi Çakmak Anadolu Lisesi**
2007 – 2011	**Atatürk Üniversitesi**
2013 –2015	**Marmara Üniversitesi**